BioNanoScience (2025) 15:557
https://doi.org/10.1007/s12668-025-02188-8

RESEARCH

Antibacterial Effect of Novel Orthodontic PEEK Beads Coated with a Conjugate of Fish Scale Hydroxy-Apatite Nanoparticles and GL13K Peptide

Harraa S. Mohammed-Salih[1] · Rana I. Mahmood[2] · Ataa Ghazi[3] · Ali Fadhil AlQrimli[4] · Taha M. Rashid[5] · Jameel R. Al-Obaidi[6,7,8] · Faridah Lisa Supian[9] · Majid S. Jabir[10]

Received: 4 June 2025 / Accepted: 16 September 2025 / Published online: 30 September 2025

Abstract

Orthodontic treatments are often associated with enamel demineralization and white spot lesions, which can lead to various processes. To address these issues, innovative materials are being explored for their antibacterial properties. This study evaluates the efficacy of newly formed orthodontic polyether ether ketone (PEEK) beads coated with hydroxyapatite nanoparticles conjugated with the GL13K-hydroxyapatite (HAP) prepared via chemical and laser methods. GL13K-HAP nanocomposites were synthesized using chemical and eco-friendly laser ablation techniques and characterized using ultraviolet-visible (UV-visible) spectroscopy, Fourier-transform infrared (FTIR), Raman spectroscopy, transmission electron microscopy (TEM), and field emission scanning electron microscopy (FESEM). The PEEK beads were coated with these nanocomposites, and their antibacterial efficacy against various bacterial strains and cytotoxicity on REF cells were assessed. Cytotoxicity was determined using the 3-(4,5-dimethylthiazol-2-yl)-2,5-diphenyltetrazolium bromide (MTT) assay, and the bactericidal effect was evaluated through the agar well diffusion assay and acridine orange/ethidium bromide (AO/EtBr) staining. The nanocomposites exhibited distinct morphological and optical properties. Coated PEEK beads prepared by both methods demonstrated significant antibacterial activity, with zones of inhibition ranging from 9 to 22 mm against bacterial strains. Cytotoxicity assays revealed biocompatibility of the coated beads, with no significant reduction in REF cell viability, highlighting their potential for clinical use. The GL13K-HAP nanocomposite coating enhanced the antibacterial properties of orthodontic PEEK beads without compromising biocompatibility, making them a promising material for reducing bacterial adhesion and preventing enamel demineralization by simply including these beads throughout all stages of fixed orthodontic treatments.

Keywords GL13K peptide · Orthodontic appliances · PEEK beads · Bacterial infection · Bio-derived nanomaterials · Fish scale biomaterial · Agricultural waste valorization

✉ Harraa S. Mohammed-Salih
dr.harraa_sabah@codental.uobaghdad.edu.iq

✉ Jameel R. Al-Obaidi
jameel@fsmt.upsi.edu.my; jr_alobaidi@yahoo.com

[1] Department of Orthodontics, College of Dentistry, University of Baghdad, Baghdad 10047, Iraq

[2] Department of Biomedical Engineering, College of Engineering, Al-Nahrain University, Jadriya, Baghdad, Iraq

[3] Department, College of Dentistry, Mustansiriya University, P.O.P., Baghdad 10052, Iraq

[4] Prosthodontics Department, Vienna Medical University, Vienna, Austria

[5] Mustansiriyah University, Baghdad, Iraq

[6] Department of Biology, Faculty of Science and Mathematics, Universiti Pendidikan Sultan Idris, Tanjong Malim, 35900 Perak, Malaysia

[7] Nanotechnology Research Centre, Faculty of Science and Mathematics, Universiti Pendidikan Sultan Idris, 35900 Tanjung Malim, Perak, Malaysia

[8] Applied Science Research Center, Applied Science Private University, Amman, Jordan

[9] Department of Physics, Faculty of Science and Mathematics, Universiti Pendidikan Sultan Idris, Tanjong Malim, 35900 Perak, Malaysia

[10] Department of Biotechnology, College of Applied Sciences, University of Technology, Baghdad, Iraq

1 Introduction

Orthodontic treatment has become an essential component of modern dentistry, significantly enhancing patients' oral health and aesthetics [1]. However, the prolonged use of fixed orthodontic appliances creates an environment conducive to bacterial colonization and biofilm formation, leading to complications such as enamel demineralization and the development of white spot lesions (WSLs) [2, 3]. Although WSLs are a recognized challenge [4, 5], this study shifts its focus toward addressing bacterial colonization, a fundamental contributor to these complications, by exploring innovative biomaterial applications to mitigate bacterial activity during orthodontic treatment [4]. Bacterial colonization on orthodontic appliances is driven by several strains, including *Streptococcus mutans*, *Staphylococcus aureus*, *Enterococcus faecalis*, and *Streptococcus sobrinus.* These microorganisms produce acids that demineralize enamel, undermining the aesthetic and functional outcomes of orthodontic therapy [6].

The selection of *S. mutans*, *S. aureus*, *E. faecalis*, and *S. sobrinus* is based on their significant roles in orthodontic-associated biofilm formation and enamel demineralization. *S mutans* is a primary cariogenic bacterium [7], while *S. aureus* frequently adheres to biomaterials in orthodontics [8]. *E. faecalis* is resilient in hostile environments, contributing to persistent infections [9], and *S. sobrinus* supports biofilm growth and acid production. While numerous in vitro and in vivo efforts have attempted to counteract these effects using antibacterial agents or materials, most conventional approaches, such as directly coating orthodontic brackets, wires, or adhesives with antibacterial nanomaterials, have shown limitations [10, 11]. Specifically, these coatings may dissipate over time, reducing their efficacy or interfering with the mechanical performance of the orthodontic appliances, compromising treatment outcomes [4, 12, 13].

These microorganisms produce acids that demineralize enamel, undermining the aesthetic and functional outcomes of orthodontic therapy [14]. The concentrations of bacteria can vary depending on the type of orthodontic material used. For instance, wires such as stainless steel (SS) and nickel-titanium (NiTi) exhibit higher biofilm adherence compared to brackets, with *S. aureus* displaying the highest concentration among tested strains [15]. While antibacterial nanomaterials have been explored to counteract these effects, conventional approaches such as coating brackets, wires, or adhesives face limitations, including dissipation over time and potential interference with the mechanical performance of orthodontic appliances [16]. Emerging strategies have also explored the incorporation of phytochemicals with antibacterial properties. These compounds, such as alkaloids, terpenoids, and polyphenols, inhibit bacterial membrane integrity, virulence factors, and biofilm formation. They also demonstrate synergistic effects with antibiotics, though further in vivo research is necessary to optimize their safety and efficacy [17]. Modifications with 10% nanotube concentrations demonstrated significant antibacterial effects against *S. mutans*, with inhibition zones of 12.50–13.20 mm, while maintaining or improving mechanical properties like compressive strength [18]. These findings underscore the need for innovative materials that combine antibacterial efficacy with long-term durability for orthodontic applications. To overcome these challenges, the present study investigates the antibacterial potential of polyetheretherketone (PEEK) beads submerged in a nano-peptide composite comprising hydroxyapatite nanoparticles (HAP) conjugated with the antibacterial peptide GL13K [19]. This innovative approach leverages the sustained release capabilities of submerged materials to maintain antibacterial activity over time without affecting the mechanical integrity of orthodontic appliances [20]. PEEK, a semi-crystalline polymer with excellent biocompatibility, mechanical strength, and resistance to wear and chemical degradation, has been widely used in biomedical applications, including dental implants. Its natural tooth-colored appearance and elastic modulus, comparable to human bone, make it a highly suitable material for orthodontic applications [21]. In recent years, PEEK has also been explored in various geometries, including disc- and bead-like configurations, to serve as experimental platforms for studying surface modifications, drug delivery, and antibacterial coating performance in dental and orthopedic applications [22, 23]. Although not yet standard in orthodontic practice, such bead-type PEEK substrates offer a controlled, reproducible model for evaluating coating adhesion and bioactivity, and they may hold future potential in the development of customizable, bioactive dental materials [24]. In this study, HAP was derived from fish scale biowaste, an economically and environmentally sustainable source, aligning with the growing interest in utilizing natural resources for biomedical applications [25, 26]. The antibacterial peptide GL13K, known for its ability to induce bacterial agglutination and inhibit biofilm formation, was incorporated into the nanocomposite to further enhance its antibacterial properties [27]. Together, these components form a biofunctional coating for PEEK beads, offering a sustainable and effective solution to bacterial colonization. Unlike direct application methods, such as coating brackets or wires, submerging PEEK beads in the nano-peptide composite provides several advantages [28]. First, it ensures a controlled and sustained release of antibacterial agents, reducing the likelihood of premature dissipation. Second,

it preserves the structural and mechanical properties of orthodontic appliances, critical for the long durations of orthodontic treatment [29]. Lastly, this approach addresses a significant gap in the current literature, as there has been limited focus on antibacterial solutions specifically designed to align with the mechanical and aesthetic requirements of orthodontics [30]. To evaluate the efficacy of this approach, the materials were characterized using advanced analytical techniques. Transmission Electron Microscopy (TEM) and Field Emission Scanning Electron Microscopy (FESEM) were employed to examine the nanocomposite's structural and surface morphology. UV-visible spectroscopy, Fourier Transform Infrared Spectroscopy (FTIR), and Raman Spectroscopy were utilized to confirm the chemical composition and functional group interactions within the material. These techniques ensured that the nanocomposite coating was successfully applied to the PEEK beads and met the necessary criteria for biocompatibility and antibacterial performance [31]. This study aims to address the challenges associated with bacterial colonization in orthodontics by introducing a novel biomaterial system designed for long-term efficacy. By integrating hydroxyapatite nanoparticles and the antibacterial peptide GL13K into a PEEK-based delivery system, this research contributes to the development of advanced biomaterials that enhance both the functional and aesthetic outcomes of orthodontic treatments. The findings are expected to provide a sustainable and effective solution to one of the most persistent challenges in orthodontic care, offering a new avenue for improving patient outcomes in the field.

2 Materials and Methods

2.1 Preparation of GL13K-HAP Nanocomposite

The nanocomposite of hydroxyapatite capping with peptide (GL13K) has been prepared by two methods: laser and chemical methods.

2.1.1 Laser Method

Laser ablation is considered one of the most interesting methods to prepare nanoparticles and is considered an eco-friendly method. the eco-friendly method, according to 0.025 g of GL13K (ChinaPeptides Co., Ltd., Shanghai, China), was dissolved in 20 ml of D.W. (solution A). A 5 g of high-purity HAP powder was placed in the pressing mould using 10 bar pressure for 10 min to get the target HAP. The target was placed in the prepared solution (solution A), and the irradiation of the laser directly focusing on the surface of HAp inside the solution with an energy of 820 mJ and a wavelength of 1064 for 600 pulses and 6 Hz. The final solution became white, and the samples were sonicated for 45 min. Then, filtered to remove large particles.

2.1.2 Chemical Method

The chemical preparation method involved the following steps: First, 0.025 g of the antibacterial peptide GL13K was dissolved in 20 mL of distilled water to create the peptide solution. Separately, 0.1 g of NaOH was dissolved in 5 mL of distilled water to prepare the alkaline solution, and 0.25 g of hydroxyapatite (HA) was dissolved in 50 mL of distilled water to form the hydroxyapatite suspension. The alkaline solution was mixed with the hydroxyapatite suspension and sonicated for 45 min to ensure uniform dispersion and to remove large particles through filtration. The resulting mixture was then combined with the peptide solution under stirring at 600 RPM for 20 min. The final product was left undisturbed overnight to allow proper settling and stabilization.

2.2 Pre-Coating: Characterization of the GL13K-HAP Nanocomposite

The morphology of the nanocomposite has been analyzed by using TEM with a magnification 77.500 Kx (ZEISS LEO 912 AB/Germany). The FESEM-EDS (ZEISS, Oberkochen, Germany) images are created by detecting reflected or knocked-off electrons. The optical properties of the nanocomposite were investigated by using UV-visible spectroscopy (Shimadzu 1900i-, Kyoto, Japan), and the vibration modes of nanomaterials were investigated using Raman spectroscopy (Malvern HORIBA, Worcester, UK). Fourier transformation of nanomaterials has been studied and investigated for the effective bonds by using FTIR (PerkinElmer, Waltham, USA).

2.3 3D-Designing and Milling of Orthodontic PEEK Beads

For the design of polyether ether ketone (PEEK) beads, the Sharp 3D program (Hungary,5.440) was used under a student account. The design started with a sketch of a circle with a diameter of 5 mm (Fig. 1A), from there a cylinder of a height of 2 mm was extruded (Fig. 1B). Then, the sharp margins of cylinder R (radius) 2.43 mm were bevelled (Fig. 1C) from the top to make it rounded and from the bottom $R = 0.5$ mm (Fig. 1(d)D). To make the middle hole, a circle of 1.05 mm diameter was sketched (Fig. 1E) to be extruded as a cylinder for subtraction for the PEEK bead. Finally, the design was exported as an STL file for milling.

In the milling process, an Arum 5x-500 milling machine (ArumDentistry, Chungcheongbuk-do, South Korea) was

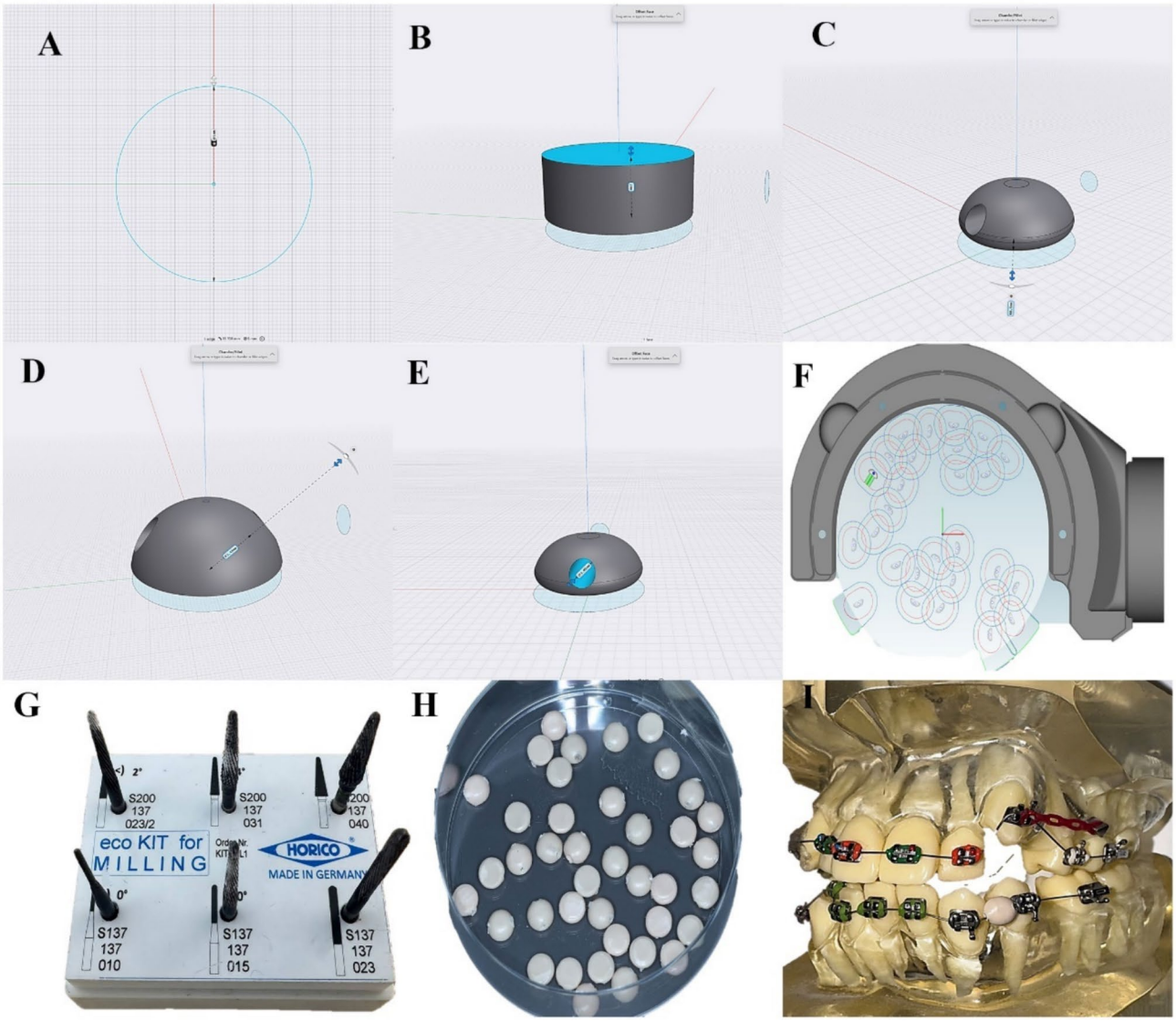

Fig. 1 The overall process of designing and milling orthodontic PEEK beads is illustrated. **A**–**E** The step-by-step CAD design process for fabricating the beads, while **F** the milling path simulation used to ensure precision manufacturing. **G** The milling tools utilized during production. **H** The fabricated PEEK beads after sterilization and preparation for testing, and **I** the application of the PEEK beads in an orthodontic setup

used, combined with hyperdent cam software (Wessling, Germany, 9.2.5). After placing the beads in the hyperdent software, only one support was on the bottom of the beads with a diameter of 2.5, which was cut to 80% after the milling process was completed (Fig. 1F). A carbide bur was used to cut out the beads and to finish the remaining parts of the support (Fig. 1G). The final form of the PEEK beads before the coating procedure is shown in (Fig. 1h). Figure 1I shows the PEEK beads sliding through the lower archwire between the brackets in an orthodontic typodont.

2.4 Coating of Orthodontic PEEK Beads with Newly Produced GL13K-HAP Nanocomposite

Following the preparation of PEEK beads, they were coated with the prepared nanocomposite on the surface, according to Liu et al. (2015) [32], with some modifications. After preparing the nanocomposite, PEEK beads were immersed in the 20 mL of both solutions of nanocomposite prepared by laser and chemical methods, as individual samples. The solution was exposed to water bath sonication for 60 min. Since the

materials contained peptides exposing them to ultrasound waves for a long time led to raising the temperature of the water; therefore, ice was placed in the water to maintain the temperature of the prepared materials. Finally, the PEEK beads were left immersed in the solution of the nanocomposite overnight. The PEEK beads were then extracted from the solution, dried, and gently cleaned to be ready to verify their applications as an antibacterial effect for three groups, which are the control group (without coating), chemical and laser.

2.5 Post-Coating: Characterization of Coated Orthodontic PEEK Beads

Using Field Emission Scanning Electron Microscopy (FESEM) (Zeiss Supra 55VP, Oberkochen, Germany), the morphology of the products was analyzed. The samples were sputter-coated with a thin layer of platinum using a sputter coating machine (Bio-Rad Polaron Division, SEM Coating System, Hercules, USA) before analysis to increase the conductivity. Also performed was Energy-Dispersive X-ray Spectroscopy (EDX). FTIR and Atomic Force Microscopy (AFM) were used to further characterize the products.

2.6 Cytotoxicity of Coated Orthodontic PEEK Beads

Cells were cultured as REF in RPMI-1640 medium, enriched with 10% fetal bovine serum, 100 units/mL of penicillin, and 100 µg/mL of streptomycin. The cells were maintained at 37 °C and reseeded twice weekly upon reaching 80% confluence [33].

The MTT assay was performed using 96-well plates to assess the cytotoxic effects of GL13K-HAp [34]. Cells were seeded at a density of 1×10^4 cells per well and treated with GL13K-HAp, either through a chemical method or laser, after 24 h or upon reaching a confluent monolayer. Following 48 h of treatment, cell viability was assessed by removing the medium, adding 100 µL of a 2 mg/mL MTT solution, and incubating the cells at 37 °C for 2.5 h. The resulting formazan crystals were dissolved in 100 µL of Dimethyl Sulfoxide (DMSO), followed by incubation at 37 °C for 15 min with shaking [35]. Absorbance was measured at 492 nm using a microplate reader, and all experiments were conducted in triplicate. The rate of inhibition (cytotoxicity percentage) was calculated using the following equation [36, 37]:-

$$\text{Inhibition rate} A = \frac{B}{A} \times 100\%$$

where A is the optical density of the control, and B is the optical density of the samples [38].

To study the morphological appearance of the cells, they were cultured in 24-well microtiter plates at a plating density of $T = 24$ h; MOI $= 1 \times 10^5$ cells/mL. The cells were centrifuged and layered into an infection solution before being incubated at 37 °C for 24 h. After incubation, the cells were subjected to GL13K-HAp via chemical processing as well as through laser for another 24 h of treatment. At the end of the treatment period, the cells were stained with crystal violet and permitted to stand at 37 °C for 10–15 min [39]. After that, the excess stain was washed off with plain tap water until no further dye came off, this was to ensure that no excess chemical was left on the tissues. Subsequently, the cells were also observed with an inverted light microscope at 100 × magnification, and the photographs were taken by attaching a digital camera to the microscope [40].

2.7 Antibacterial Activity and Detection of Live and Dead Bacterial Cells

The powder was prepared according to Muller-Hinton (M-H) by adding 20 mL of the powder to 1L of distilled water, then heating on a burner by shaking. For sterilization, M-H must be autoclaved at 121 °C for 15 min. It was allowed to cool to 50 °C and then poured into a petri dish. After that, it was left in solidification for around 15 min and then flipped upside down, and placed into the refrigerator at 4 °C. The antibacterial potential of the prepared samples (Control, Laser, and Chemical) was determined against Gram's negative and Gram's positive bacteria using an agar well diffusion assay [33]. Sterile Petri dishes were used for each of which about 20 mL of MH agar was aseptically poured. The stock cultures of the bacterial species were used to gather each bacterial species using a sterile wire loop. The organisms were cultured and then, using a sterile tip, they were bored into 6 mm diameter wells on the agar plates. Other concentrations of samples were used in the bored wells. The average zones of inhibition diameter were measured and recorded [41] after cultured plates containing samples and test organisms were incubated overnight at 37 °C.

An Acridine orange-ethidium bromide (AO/EtBr) staining procedure was used for cell viability detection in an experiment. The antibacterial activity of the products was measured using a fluorescent microscope (Olympus, Japan). Fifty microliters of bacterial suspension of both the treated and untreated was mixed with 50 µL of the AO/EtBr, and left for 2 min. After staining, the mixture was applied onto a glass slide, and a thin film of the mixture was observed under an immunofluorescent microscope (Olympus, Japan). The living cells fluoresced green with Acridine orange, and the dead cells fluoresced red with ethidium bromide.

2.8 Statistical Analysis

Data were statistically analysed using the GraphPad Prism program. The collected data of cytotoxicity percentage and antibacterial values were expressed by descriptive statistics as the

mean ± standard deviation (SD) based on triplicate measurements. Antibacterial data were furtherly inferentially analysed which conducted on inhibition zone data from three experimental groups (Control, Laser, Chemical) tested against four bacterial species. The analysis includes assumption checks by Shapiro-Wilk test, a two-way ANOVA, and post hoc comparisons using Tukey's HSD. Indicate statistically significant difference at $p < 0.05$. Details of the sample size calculation and group distribution are provided in Supplementary Figure S1.

3 Results

3.1 Pre-Coating: Characterization of the Nanocomposite GL13K-HAP

The optical, structural, and morphological of the GL13K, HAP, GL13K-HAP by laser method, and GL13K-HAP by chemical method nanocomposite have been characterized by using UV-visible spectroscopy, FTIR, Raman spectroscopy, TEM, and FESEM-EDS.

3.1.1 UV-Visible Spectroscopy

UV-visible spectroscopy of GL13K, HAP, GL13K-HAP by the laser method, and GL13K-HAP by the chemical method is represented in Fig. 2. Because HAP has no detectable specific absorption band in the visible range, its inherent optical stability is evidenced. This observation is important as it guarantees the structural integrity of the nanocomposite under various lighting conditions, thus enabling long-term orthodontic applications. Furthermore, the spectral behaviour of GL13K-HAP conjugated by both methods suggests that conjugation has been accomplished, which may improve the antibacterial efficacy of the conjugate.

3.1.2 FTIR Spectroscopy

The topography shown in Fig. 9 is the surface roughness profile of the topography of the chemical and laser methods. The increased roughness observed in the chemically prepared GL13K-HAP (Ra: 35. Enhanced surface activity was indicated by comparison to the laser method (Ra, 27.50 nm) (47 nm) (Fig. 3). In this case, this rougher profile might serve better in providing better antibacterial properties, i.e., disrupting bacterial adhesion that is important for orthodontic applications. Further, the better biocompatibility afforded by the smoother surface of the laser method would facilitate the irritation of oral tissue. The versatility of these different coating approaches is reflected in these distinct profiles, which will be tuned according to clinical needs.

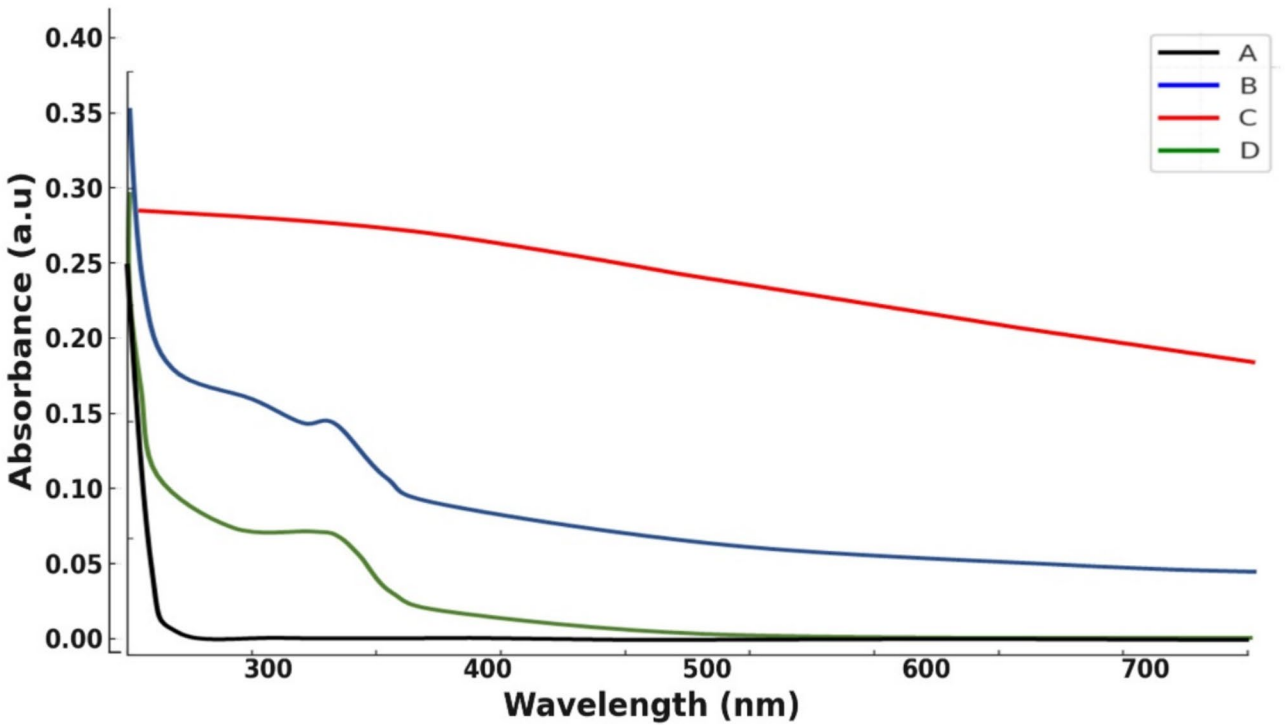

Fig. 2 UV-Visible spectroscopy of **A** HAP, **B** GL13K, **C** GL13K-HAP by laser method, and **D** GL13K-HAP by chemical method

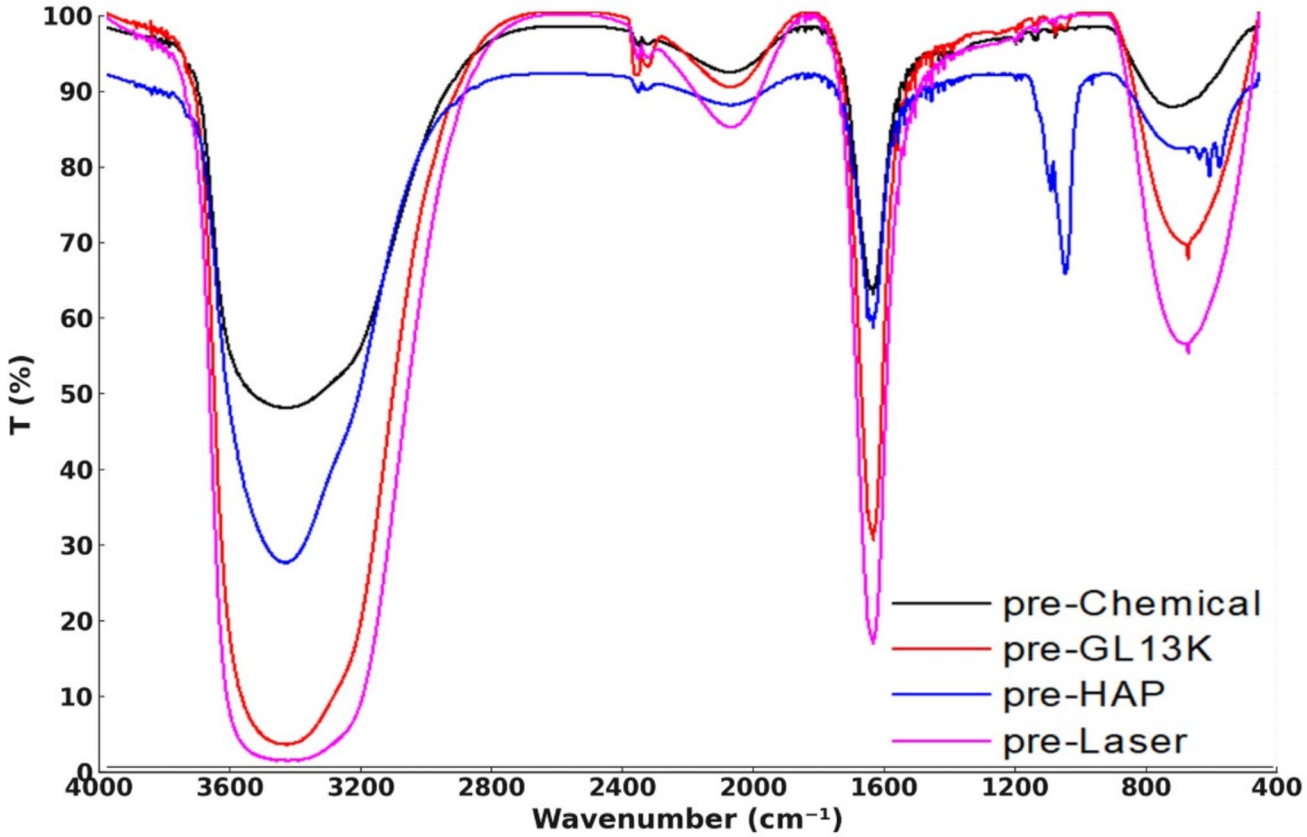

Fig. 3 FTIR spectroscopy of **A** HAP, **B** Gl13K, and **C** GL13K-HAP by laser method, and **D** GL13K-HAP by chemical method

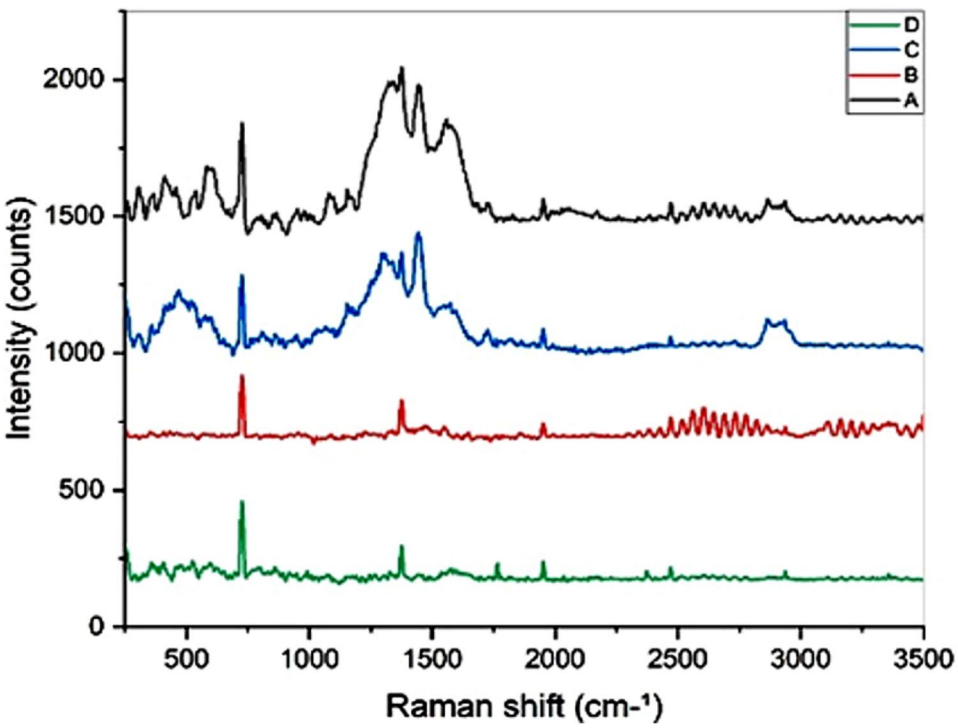

Fig. 4 Raman spectroscopy of **A** GL13K, **B** HAP, and **C** GL13K-HAP by laser method, and **D** GL13K-HAP by chemical method

3.1.3 Raman Spectroscopy

Results from the Raman spectroscopy (Fig. 4) indicated successful conjugation of GL13K with HAP due to the clear shift at 750 cm^{-1} for C-C and additional CH_2 peaks in GL13K-HAP. This structural change suggests that the peptide/hydroxyapatite interaction has increased, potentially providing the basis for improved antibacterial properties. Additional CH_2 peaks also point to increased hydrophobicity, which may facilitate the disruption of the bacterial membrane. Additionally, these findings add further confirmation of the suitability of the nanocomposite for orthodontic use.

3.1.4 TEM Analysis

The TEM analysis, as shown in Fig. 5, highlights the differences in particle size and morphology across the nanocomposites. Sample A (HAP) exhibited highly aggregated and irregularly shaped particles with a mean particle size (MPS) of 57.5 nm, consistent with the clustering tendency of hydroxyapatite nanoparticles. In contrast, Sample B (GL13K) showed smaller and more dispersed particles with an MPS of 51 nm, likely due to the stabilizing effect of its peptide-based molecular structure. For Sample C (GL13K-HAP by laser method), the nanoparticles were well-dispersed, spherical, and had the smallest MPS of 48 nm, demonstrating the laser method's effectiveness in reducing aggregation and improving uniformity. Sample D (GL13K-HAP by chemical method) also exhibited a uniform morphology, with a slightly larger MPS of 53.1 nm and mild aggregation, reflecting effective control by the chemical method but less precision compared to the laser method. Overall, the laser method produced the smallest and most uniform particles, which may enhance surface interactions and biological activity for biomedical applications.

3.1.5 Morphological Analysis by FESEM-EDS

The morphologies of the HAP, GL13K, and GL13K-HAP by the chemical method and laser are shown in Fig. 6. The FESEM analysis revealed distinct differences in particle sizes and distributions across the samples. The smaller particle sizes observed in GL13K-HAP synthesized via the laser method (50–70 nm) compared to the chemical method (20–40 nm) highlight the precision and consistency of the laser approach. Smaller particles generally provide a higher surface area, enhancing interactions with bacterial cells and potentially increasing antibacterial efficacy. The EDS results further confirm the compositional integrity of the samples, with the laser method showing fewer impurities, underscoring its eco-friendly advantages.

3.2 Post-Coating: Characterization of Coated Orthodontic PEEK Beads

The nanocomposite-coated PEEK beads are coated separately by GL13K-HAP nanocomposite, which was prepared by using the chemical method and the laser method. They were characterized by using FESEM-EDS, FTIR, and AFM.

3.2.1 Morphological Analysis: FESEM-EDS Post-coating

Post-coating FESEM-EDS analysis indicated significant differences between the chemical and laser methods (Fig. 7). The chemical method resulted in more uniform coverage with particle sizes of 30–50 nm, which can enhance bacterial resistance. Conversely, the laser method produced a more heterogeneous coating with smaller particle sizes (20 nm), which may improve mechanical integration and reduce bacterial adhesion. The presence of elements like Ti and P in the chemical coatings also suggests potential interactions with enamel or dentin surfaces, providing an additional layer of functionality.

3.2.2 FTIR Comparison

Key differences in the chemical bonding of coatings prepared using laser and chemical methods were observed from FTIR spectra. Laser preparation appears more effective for strengthening the O-H and N-H bonding signals indicative of stronger hydrogen bonding, and hence possibly improved material stability and biocompatibility (Fig. 8). The chemically prepared samples show an enhanced C=O stretch that is indicative of greater peptide conjugation, which may aid antibacterial activity. These results indicate that the synthesis method can be tuned to achieve desired properties, suitable for clinical needs.

3.2.3 AFM and Surface Roughness Assessment: Post-coating Results

The AFM analysis revealed that the chemically prepared GL13K-HAP had higher surface roughness (Ra: 35. A comparison of the laser method (Ra, 27.50 nm) with the method using the ion beam (Ra: 27.25 nm and 22.40 nm, respectively, for radius defined as, respectively, the mean and the standard deviation). It is advantageous for bacterial disruption, but it increases wear slightly under dynamic conditions. Laser preps appear to be smoother than mechanically prepared ones, and may provide for better integration of oral tissues with less irritation and better long-term biocompatibility (Fig. 9). The findings emphasise the need to optimise the combination of surface roughness and performance for the application. The surface roughness profile is displayed

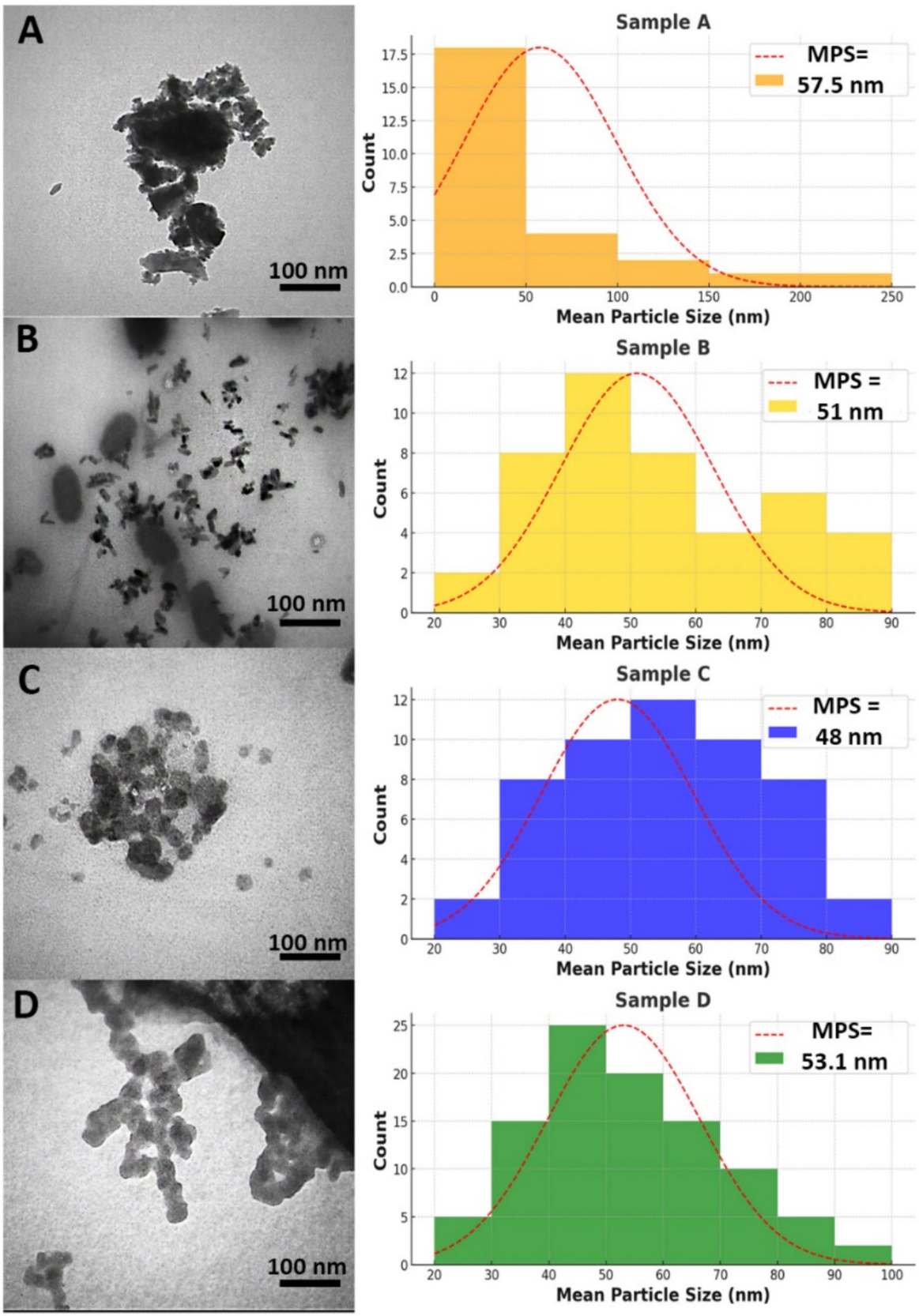

Fig. 5 The TEM result of **A** HAP, **B** Gl13K, and **C** GL13K-HAP by laser method, and **D** GL13K-HAP by chemical method

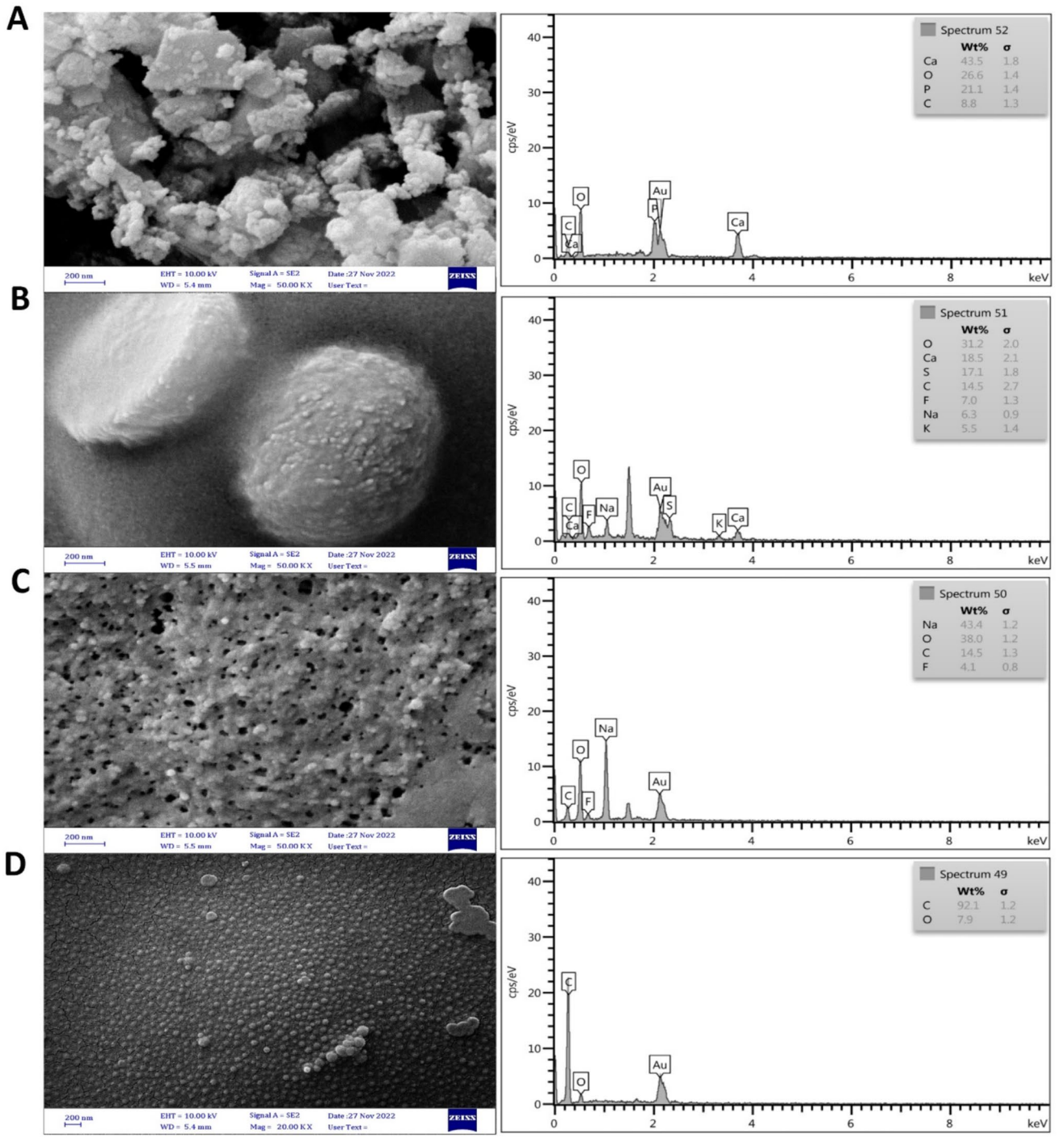

Fig. 6 FESEM-EDS analysis of **A** HAP, **B** GL13K, and **C** GL13K-HAP by chemical method, and **D** GL13K-HAP by laser method

in Fig. 9 of the (A) chemical and (B) laser methods topography of the height parameter. The average roughness parameter values (Ra) are tabulated as 35.47 nm for chemical and 27.50 nm for laser, respectively, as the standard deviation of all the height values (Table 1) that describe the overall surface roughness, in which the surfaces are relatively smooth with subtle diffraction peaks [42]. The height distribution relative to the mean line is Rq = 51.23 nm (38.74 nm), respectively. The rougher GL13K-HAP using a chemical is rougher than laser, with average maximum peak-to-valley height or maximum roughness values consistent with Ra values. They both come out with similar results.

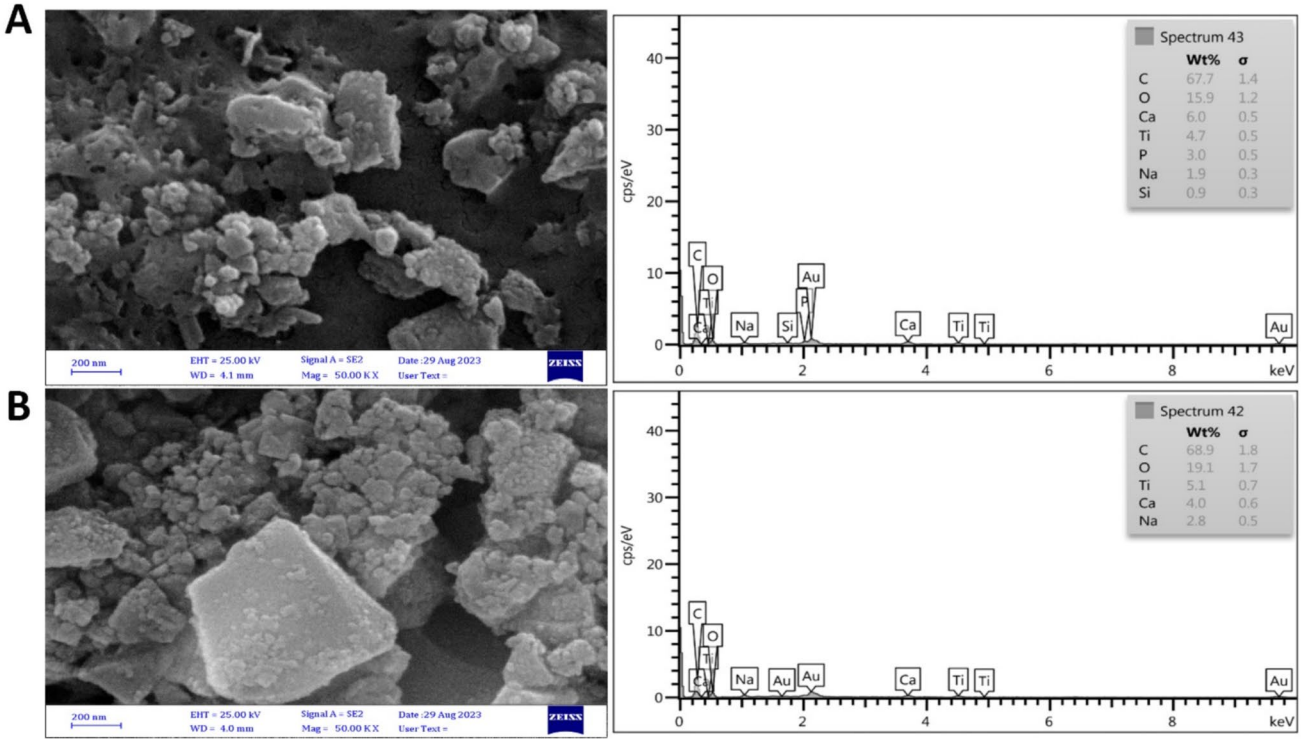

Fig. 7 FESEM-EDS analysis of Orthodontic PEEK beads post-coating by GL13K-HAP **A** chemical method and **B** laser method

3.3 Cytotoxicity of Coated Orthodontic PEEK Beads

The cytotoxic effect of GL13K-HAP by the laser method and GL13K-HAP by the chemical method against REF cells was studied. The antiproliferative activity of GL13K-HAP by the laser method and GL13K-HAP by the chemical method was tested by studying their ability to inhibit the proliferation of the REF cell line. The cytotoxicity percentage results of this study are shown in Figs. 10 and 11. The results demonstrated that the prepared GL13K-HAP by the laser method and GL13K-HAP by the chemical method are biocompatible with the REF cell line.

3.4 Antibacterial and Detection of Live and Dead Bacterial Cells

The antibacterial efficacy of GL13K-HAP coatings was evaluated against *S. mutans, S. aureus*, *E. faecalis*, and *S. sobrinus* (Figs. 12, 13, 14, 15, and 16). Both the laser (Sample B) and chemically synthesized (Sample C) nanocomposites demonstrated significant inhibition zones, with the chemically synthesized coating consistently showing the largest zones of inhibition across all strains.

For *S. mutans* (Fig. 13), the inhibition zones were 17.6 ± 0.47 mm (Sample C) and 15.8 ± 0.62 mm (Sample B). Similarly, against *S. aureus* (Fig. 14) and *E. faecalis* (Fig. 15), Sample C exhibited zones of 21.0 ± 0.81 mm, compared to 18.8 ± 0.84 mm and 17.3 ± 0.94 mm for Sample B. For *S. sobrinus* (Fig. 16), Sample C again outperformed Sample B, with inhibition zones of 12.4 ± 0.29 mm and 8.5 ± 0.40 mm, respectively. All data analysis was summarized in Table 2.

The radar chart (Fig. 12) illustrates the overall antibacterial activity, with the chemically synthesized nanocomposite covering the largest area, followed by the laser method. The control (Sample A) showed no activity. These results confirm the effectiveness of GL13K-HAP coatings in reducing bacterial colonization and preventing orthodontic-associated infections.

The results of inferential statistical analysis were conducted on inhibition zone data from three experimental groups (Control, Laser, and Chemical) tested against four bacterial species. Shapiro-Wilk Test for normality check showed that most groups passed normality ($p > 0.05$). The homogeneity of variance is violated using Levene's Test $= 7.59$, ($p = 0.0019$).

The ANOVA results showed significant effects ($p \leq 0.05$) of both the coating method and bacterial species on inhibition zones, as well as a significant interaction between them, as shown in Table 3.

In Table 4, Tukey's post hoc analysis revealed that for all bacteria, both Laser and Chemical groups had significantly greater inhibition zones than Control. Chemical coating generally outperformed Laser, especially for *E. faecalis*

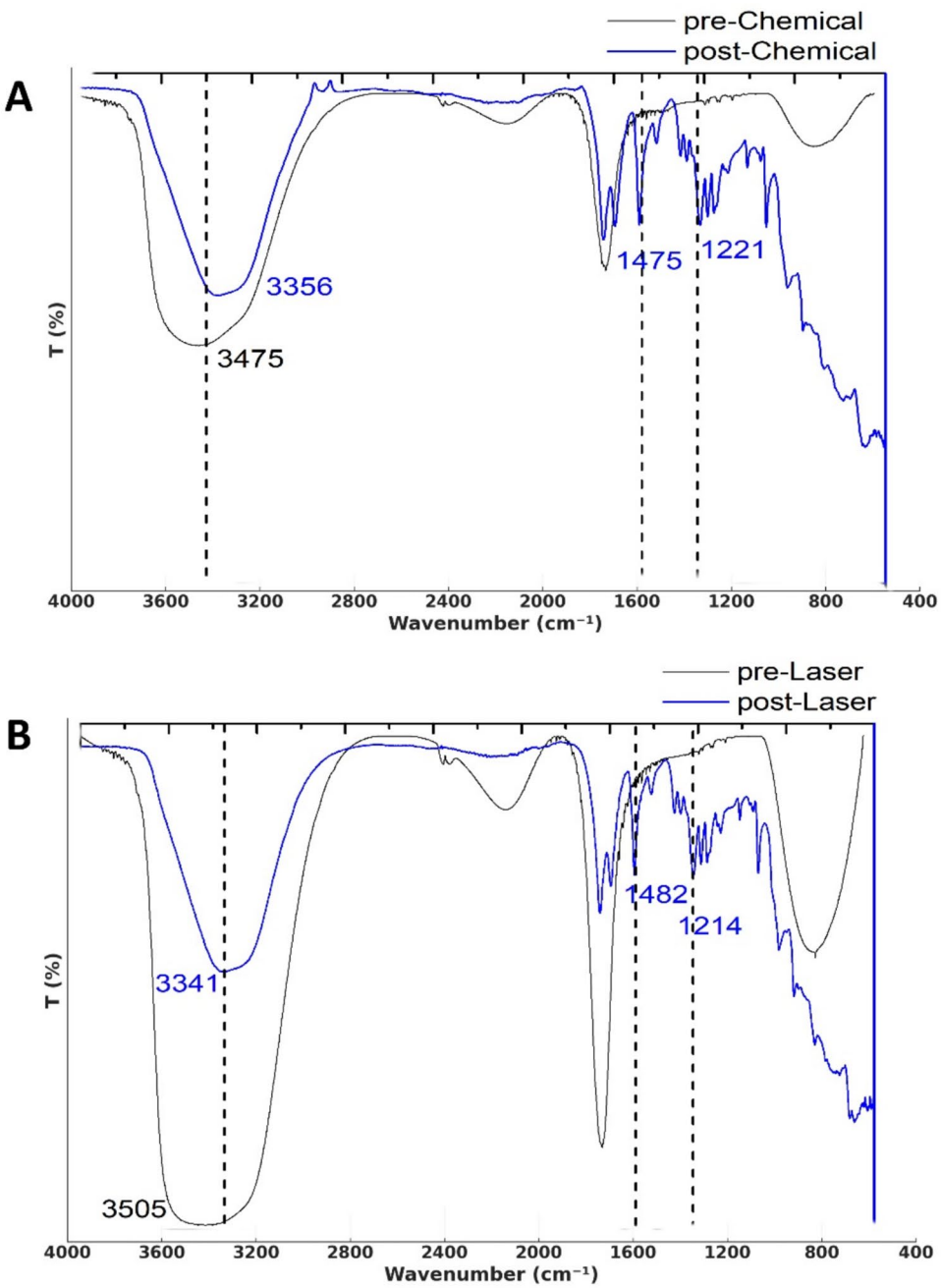

Fig. 8 FTIR comparison of Orthodontic PEEK beads post-coating by GL13K-HAP **A** chemical method and **B** laser method

and *S. mutans*. No overlap in inhibition zones was observed between Control and the two coated groups, confirming the antibacterial effect of the GL13K-HAP coatings.

3.5 GL13K-HAP Induce Production of ROS

Reactive oxygen species (ROS) were analyzed in bacterial strains treated with GL13K-HAP, made by chemical and laser means, using the AO/EtBr staining technique. This technique detects ROS via nitric oxide and EtBr interactions as oxidative stress or damage within the organism. EtBr is a selectively permeant component that binds to nucleic acids, which will enter cells with damaged membrane integrity. This causes red staining for dead cells, and green for viable cells. Cellular structures of bacterial strains treated with GL13K-HAP showed greater structural deformities and ROS levels compared to the untreated cells (Fig. 17). EtBr penetration was only allowed into cells with damaged membranes, confirming that cells with the most damage and oxidative stress in the treated samples were stained.

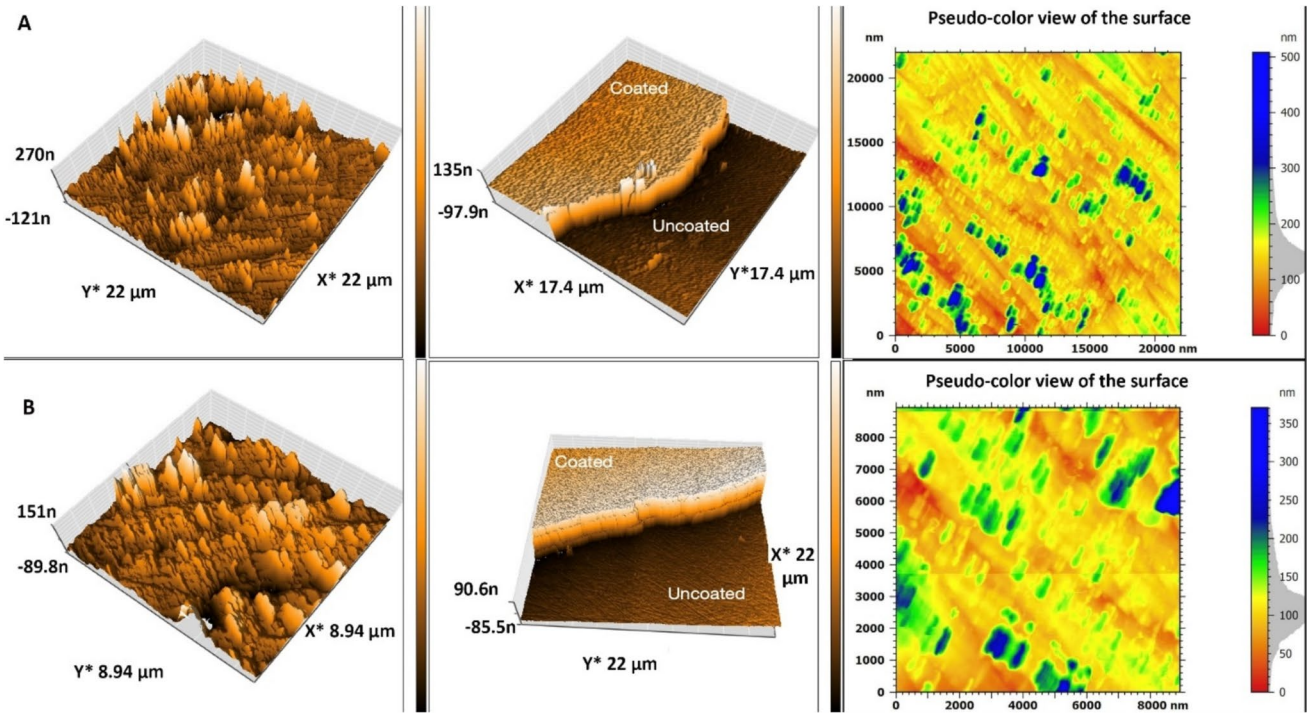

Fig. 9 AFM analysis of orthodontic PEEK beads post-coating by GL13K-HAP **A** chemical method and **B** laser method

4 Discussion

4.1 Pre-Coating: Characterization of the nanocomposite GL13K-HAP

The optical, structural, and morphological properties of GL13K, HAP, and GL13K-HAP nanocomposites synthesized using chemical and laser methods were thoroughly characterized. These analyses revealed distinct features that highlight the potential of these nanocomposites for biomedical applications. UV-visible spectroscopy demonstrated that HAP exhibited no specific absorption band in the visible range, confirming its inherent optical stability. This stability was retained in GL13K-HAP nanocomposites prepared by both chemical and laser methods, as evidenced by their optical transparency. Such properties are advantageous for biomedical coatings, where transparency and structural integrity are critical for effective performance [43].

Table 1 Sample group film values of the average roughness (Ra), root mean square roughness (Rq), and average maximum roughness (Rz)

GL13K-HAP	Ra (nm)	Rq (nm)	Rz (nm)
Chemical	35.47	51.23	507.9
Laser	27.50	38.74	370.6

FTIR spectroscopy provided deeper insights into the molecular structure of the nanocomposites. Broad bands between 3200 cm^{-1} and 3600 cm^{-1} corresponded to O-H bonds, while the sharp peak at 1644 cm^{-1} indicated the presence of C=O amide groups, essential for peptide functionality [44]. The transmittance in the range from 2100 cm^{-1} to 2500 cm^{-1} corresponded to C=C and C≡C [45, 46]. Furthermore, C=C and C≡C stretching between 2100 cm^{-1} and 2500 cm^{-1} highlighted the structural diversity of the GL13K-HAP composite. Interestingly, the distinct transmittance at 1040 cm^{-1} in pre-HAP, corresponding to the C-N bond, was absent in GL13K-HAP, suggesting that the conjugation process altered the molecular structure. These transformations provide a range of functional groups critical for applications such as adhesion and bonding to biological surfaces. These findings, collectively, suggest that despite the chemical inertness of PEEK, the functionalization by laser or chemical methods facilitates sufficient bonding through hydrogen bonding, hydrophobic interactions, and mechanical interlocking. Compared to previous studies using pure hydroxyapatite coatings [47], the incorporation of GL13K peptide into the nanocomposite significantly enhanced antibacterial efficacy, as evidenced by larger inhibition zones (17.6 ± 0.47 mm vs. 12 mm). This highlights the synergistic effect of peptide conjugation in disrupting bacterial adhesion. Additionally, laser synthesis offers distinct advantages,

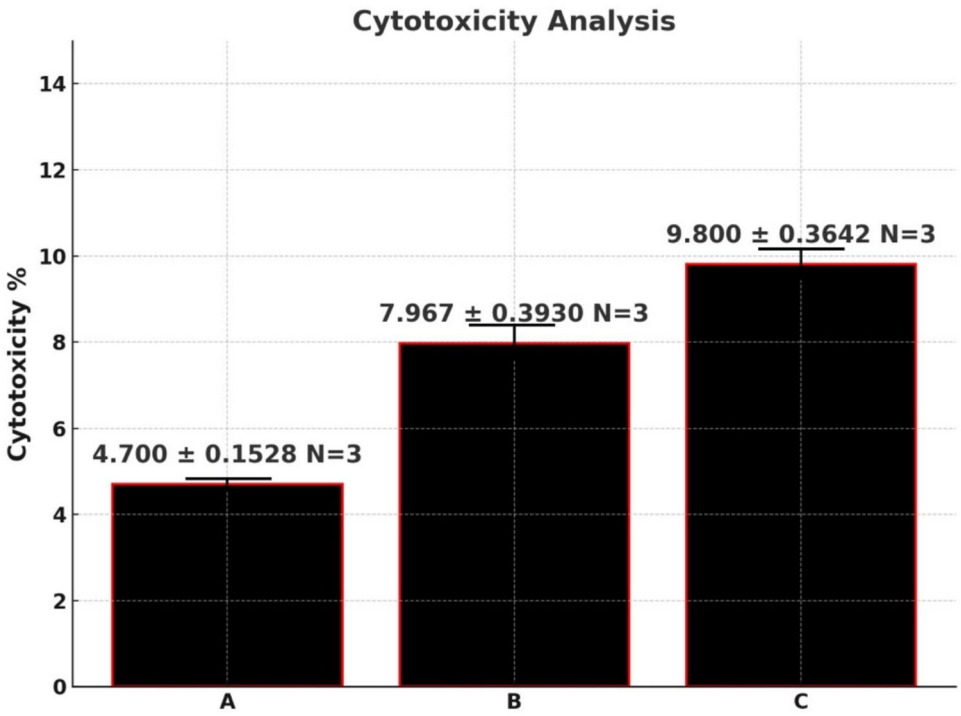

Fig. 10 Biocompatibility of orthodontic PEEK beads post-coating by GL13K-HAP in REF cells. A) control, B) laser method, C) chemical method

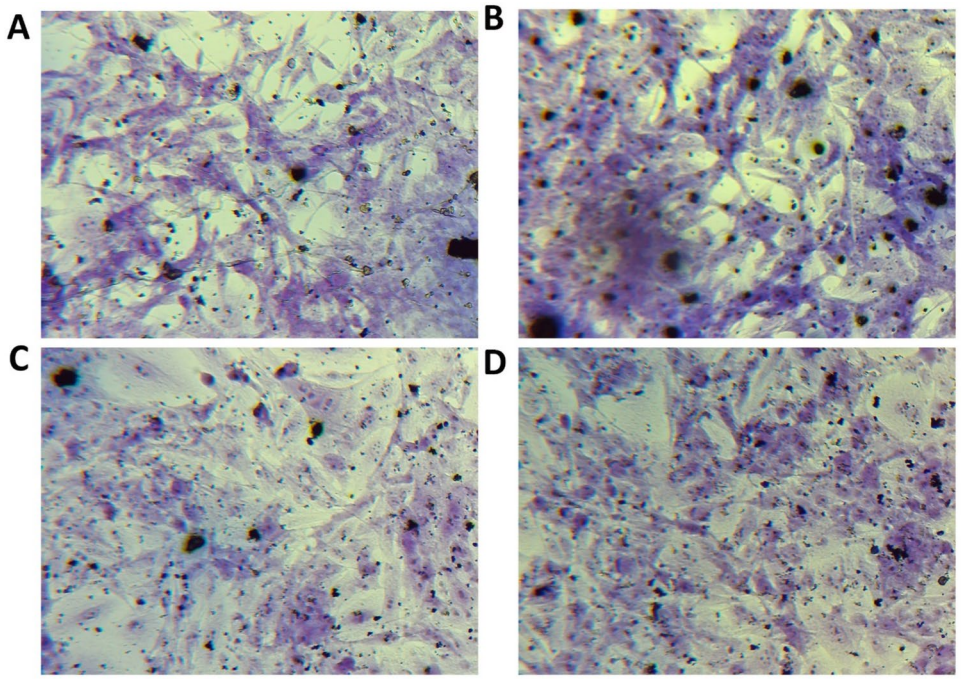

Fig. 11 **A** REF untreated cells and **B** REF cells after being treated with control beads. **C** REF cells after being treated with laser-prepared GL13K-HAP beads. **D** REF cells after being treated with chemically prepared GL13K-HAP beads

producing smaller, more uniform particles compared to traditional methods reported in earlier literature [48].

Based on Fig. 4, all samples showed a Raman shift at 750 cm^{-1}, which indicated the presence of C-C [49]. GL13K and GL13K-HAP demonstrated an obvious shift from 1300 cm^{-1} compared to HAP and GL13K-HAP, assigning the CH_2 [50]. However, Gl13K and GL13K-HAP showed extra CH_2 before 3000 cm^{-1}, even though it is not observed in HAP and GL13K-HAP [51]. These findings highlight the unique molecular dynamics introduced by the GL13K component, which likely enhances the flexibility and functionality of the composite, making it more suitable for biomedical applications.

High-resolution nanoscale imaging through TEM, as shown in Fig. 5, provided critical insights into particle size

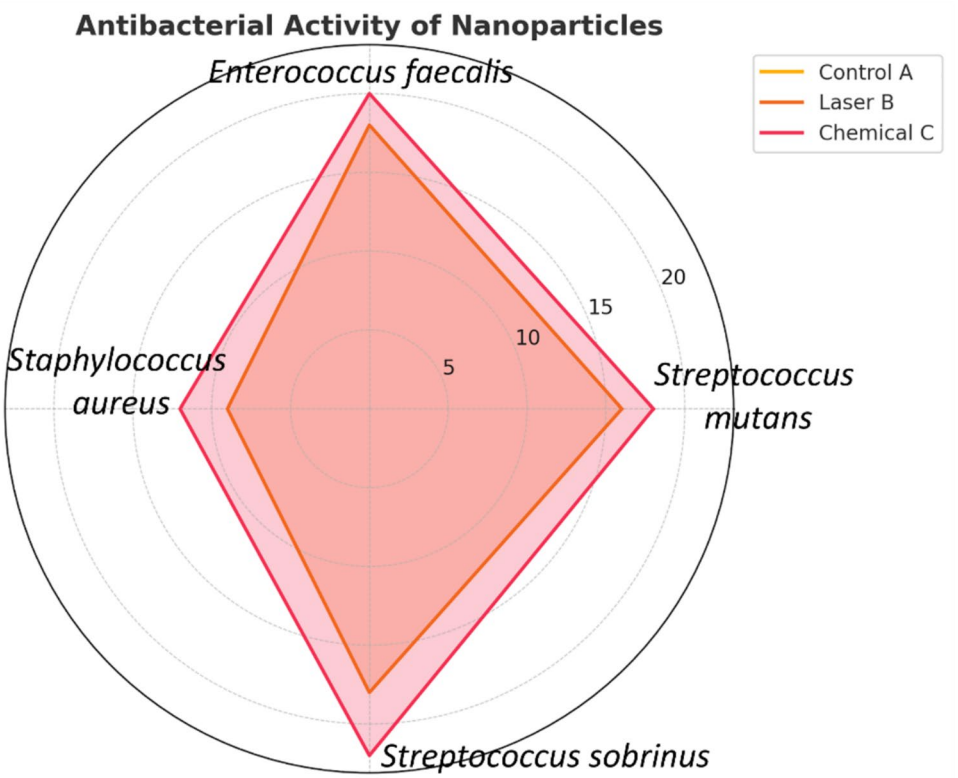

Fig. 12 The antibacterial activity of orthodontic PEEK beads post-coating by GL13K-HAP nanocomposites, A) Control, B) Laser method, C) Chemical method

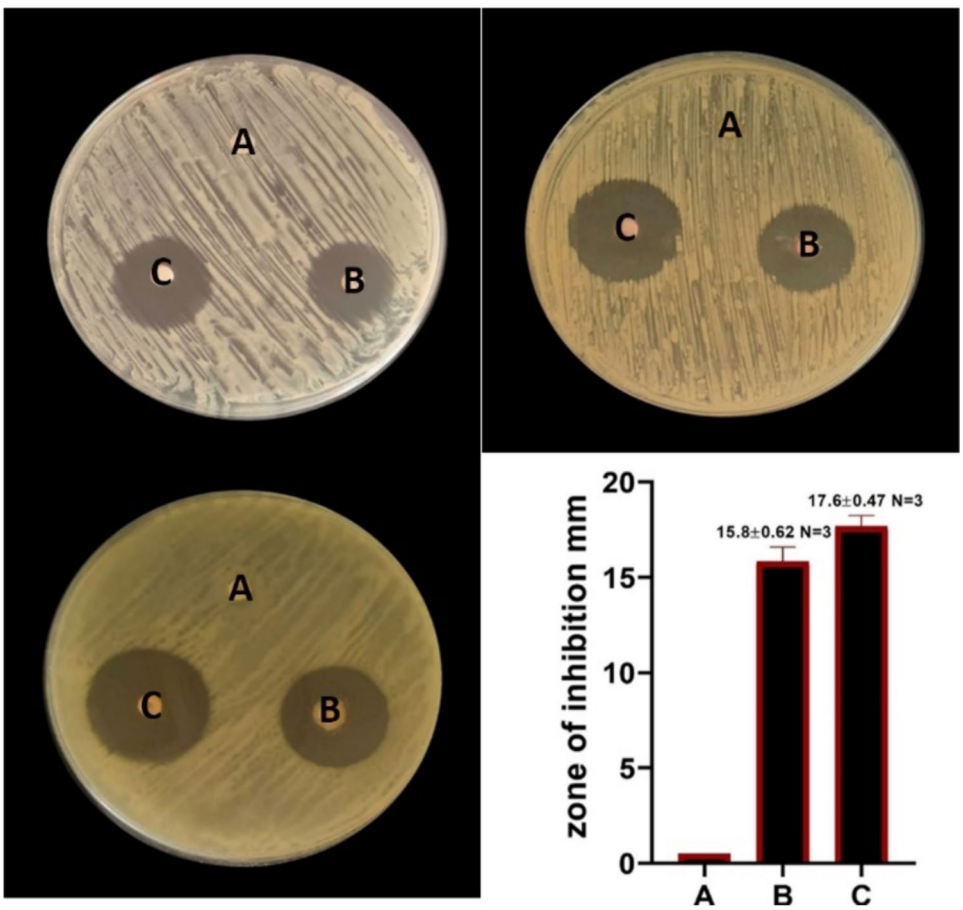

Fig. 13 Antibacterial activity of orthodontic PEEK beads post-coating by GL13K-HAP nanocomposites A) control, B) laser method, C) chemical method against *S. mutans*

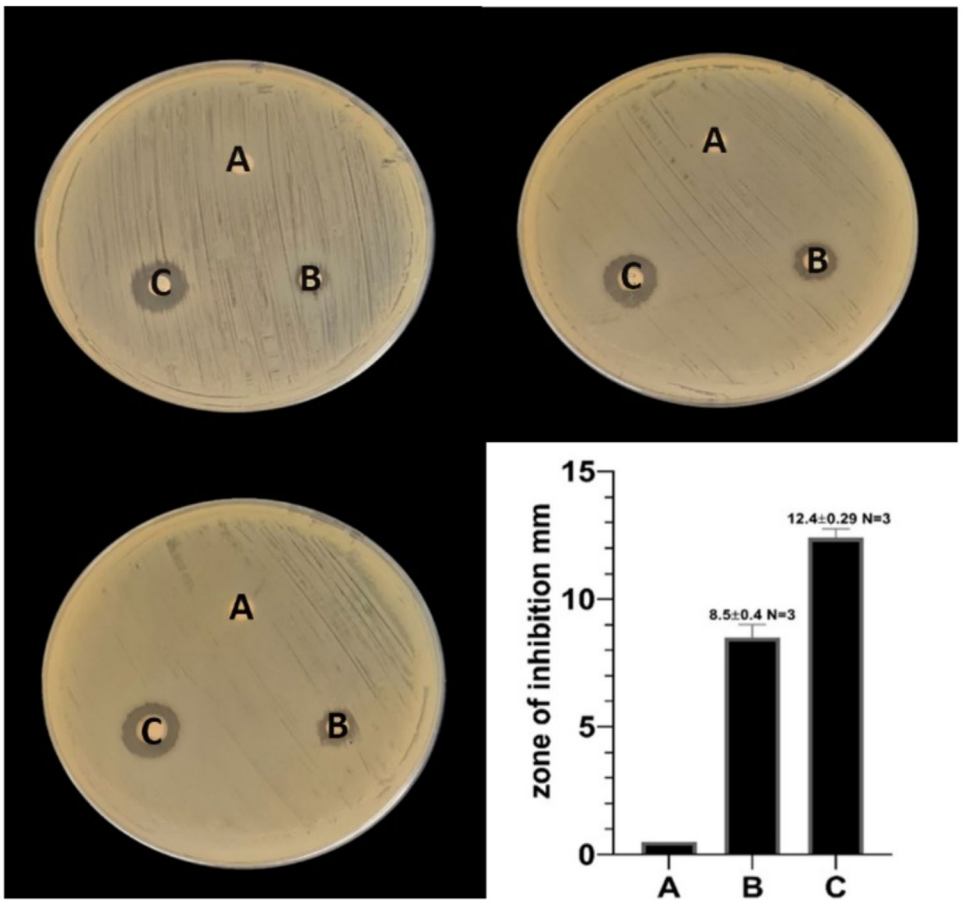

Fig. 14 Antibacterial activity of orthodontic PEEK beads post-coating by GL13K-HAP nanocomposites A) control, B) laser method, C) chemical method against *S. aureus*

distribution for each sample. TEM's ability to visualize nanoparticles at nearly atomic resolution allowed for accurate measurement of the mean particle sizes [52]. Among the samples, HAP exhibited the largest particle size, followed by GL13K-HAP and GL13K. GL13K-HAP demonstrated the smallest particle size, which is advantageous in biomedical applications as smaller particles offer a higher surface area. This increased surface area enhances biological activity, facilitates better interactions with cells, and improves antibacterial efficacy [53].

The smaller particle sizes observed in the laser-prepared GL13K-HAP nanocomposites may increase their surface area, facilitating more effective bacterial membrane disruption. Additionally, the unique molecular dynamics introduced by the CH_2 peaks in GL13K enhance the composite's hydrophobicity, potentially improving its ability to destabilize bacterial adhesion sites. These properties together may explain the enhanced antibacterial activity observed in the laser-prepared samples [54].

FESEM-EDS analysis revealed distinct morphological and elemental characteristics of the nanocomposites. Figure 6A depicts the FESEM image of HAP, showing particles of varying sizes and shapes with elements such as Ca, O, P, and C identified. In Fig. 6B, additional elements such as O, Ca, S, C, F, Na, and K were detected, reflecting the diversity of GL13K-HAP synthesized via chemical methods. Figure 6C shows that the particle sizes of GL13K-HAP prepared chemically ranged between 20 and 40 nm at a magnification of 50 K. EDS analysis confirmed the presence of Na, O, C, and F for chemically synthesized samples, whereas only C and O were detected in the laser-prepared composites. On the other hand, the FESEM image in Fig. 6D revealed that GL13K-HAP prepared by the laser method had a more uniform distribution of particles with sizes ranging from 50 to 70 nm [55].

4.2 Post-Coating: Characterization of Coated Orthodontic PEEK Beads

The nanocomposite-coated PEEK beads of two groups are coated by nanocomposite using the chemical method and laser method. They were characterized by using FESEM-EDS, FTIR and AFM. FESEM-EDS analysis revealed the morphological differences and elemental composition of the GL13K-HAP coatings post-coating, as shown in Fig. 7. The FESEM image in Fig. 7(a)A depicts GL13K-HAP particles synthesized via the chemical method, with particle sizes ranging between 30 and 50 nm at a magnification of 50 K. EDS

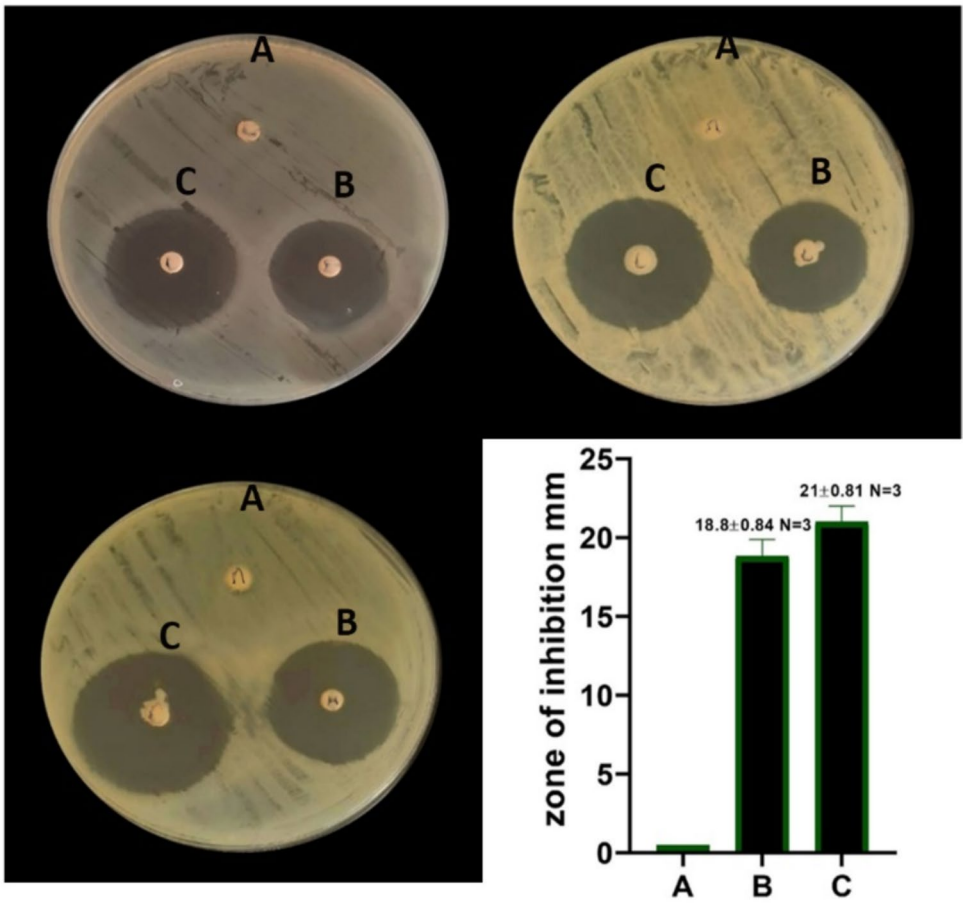

Fig. 15 Antibacterial activity of orthodontic PEEK beads post-coating by GL13K-HAP nanocomposites A) control, B) laser method, C) chemical method against *E. faecalis*

analysis confirmed the presence of elements such as C, O, Ca, Ti, P, and Na in the chemically synthesized coatings, while the laser method resulted in fewer detectable elements, specifically C, O, Ti, Ca, and Na [56]. Conversely, Fig. 7(b)B demonstrates that laser-synthesized particles were smaller, with sizes around 20 nm. The presence of Ca, Ti, and Na in the chemically synthesized nanocomposites suggests their potential to enhance bioactivity, particularly through the synergistic promotion of osteogenic responses during orthodontic treatments. Meanwhile, the smaller particle sizes resulting from laser coating could reduce friction and provide smoother surfaces, advantageous for minimizing wear in dynamic oral environments [57].

FTIR analysis of GL13K-HAP coatings highlighted key differences in chemical bonding between the two synthesis methods. Transmittance spectra (Fig. 8) revealed strong signals between 3300 cm^{-1} and 3500 cm^{-1} in both methods, corresponding to O-H and N-H stretching. Notably, the laser method exhibited more pronounced differences in transmittance spectra, reflecting variations in the distribution of chemical bonds [58]. Additional peaks between 1400 cm^{-1} and 1210 cm^{-1} indicated the presence of C=O stretching bonds. These spectral variations suggest that the synthesis method influences the chemical bond strength and distribution, potentially affecting the long-term adhesion and wear resistance of the coatings under dynamic conditions in the oral cavity.

4.3 Cytotoxicity of Coated Orthodontic PEEK Beads

The cytotoxicity assessment of GL13K-HAP-coated orthodontic PEEK beads demonstrated excellent biocompatibility for both chemical and laser-prepared materials [59]. The MTT assay results indicated minimal inhibition of REF cell growth, with cell viability consistently exceeding 85% across all tested concentrations. This confirms that the nanocomposite coatings did not induce significant cytotoxic effects, a crucial requirement for clinical applications in orthodontics [60]. These results suggest that GL13K-HAP coatings can effectively address key challenges in orthodontics, such as bacterial colonization and associated enamel demineralization. The biocompatibility of laser-prepared coatings, combined with their antibacterial activity, positions them as an ideal material for long-term orthodontic treatments, particularly in pediatric patients or for individuals with prolonged treatment durations. The eco-friendly synthesis process further enhances its appeal for scalable clinical use [61].

The high degree of biocompatibility observed is likely due to the natural origin of hydroxyapatite and the bioactive

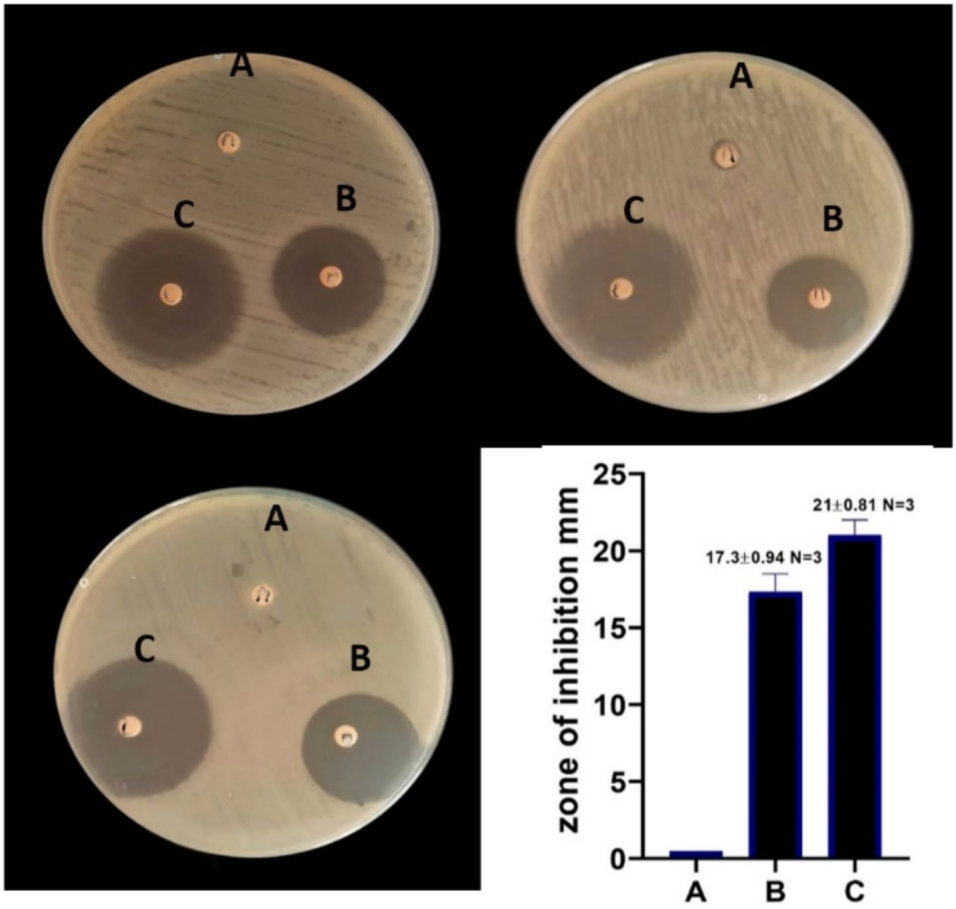

Fig. 16 Antibacterial activity of orthodontic PEEK beads post-coating by GL13K-HAP nanocomposites A) control, B) laser method, C) chemical method against *S. sobrinus*

Table 2 Descriptive statistics of inhibition zones (mm) by bacterial type and coating group

Bacteria type	Group	*N*	Mean	SD	Min	Max
S. mutans	Control	3	0.00	0.00	0.00	0.00
	Laser	3	15.83	0.62	15.00	16.50
	Chemical	3	17.67	0.47	17.00	18.00
S. aureus	Control	3	0.00	0.00	0.00	0.00
	Laser	3	8.50	0.40	8.00	9.00
	Chemical	3	12.40	0.29	12.00	12.70
E. faecalis	Control	3	0.00	0.00	0.00	0.00
	Laser	3	18.83	0.84	18.00	20.00
	Chemical	3	21.00	0.81	20.00	22.00
S. sobrinus	Control	3	0.00	0.00	0.00	0.00
	Laser	3	17.33	0.94	16.00	18.00
	Chemical	3	21.00	0.81	20.00	22.00

Table 3 Two-way ANOVA results showing the effects of coating group, bacterial species, and their interaction on inhibition zone diameter (mm)

Source	*F*-value	*p*-value	Significance
Group	2359.65	2.8156e-28	Significant
Bacterial type	155.23	7.5633e-16	Significant
Group: Bacterial type	40.52	2.1176e-11	Significant

properties of the peptide, both of which align well with the physiological environment of oral tissues. Notably, laser-prepared GL13K-HAP exhibited slightly lower cytotoxic effects compared to its chemically prepared counterpart. This distinction can be attributed to the absence of residual chemicals in the laser synthesis process, which reduces potential toxicity [62]. Consequently, laser-prepared coatings may offer a safer alternative for clinical applications, particularly

Table 4 Tukey's post hoc comparisons identifying significant differences in inhibition zones between treatment groups for each bacterial species ($p \leq 0.05$)

Bacteria	Group	Mean difference	*p*-value
S. mutans	Control vs laser	15.83	0.0000
	Control vs chemical	17.67	0.0000
	Laser vs chemical	1.83	0.0156
S. aureus	Control vs laser	8.50	0.0000
	Control vs chemical	12.40	0.0000
	Laser vs chemical	3.90	0.0000
E. faecalis	Control vs laser	18.83	0.0000
	Control vs chemical	21.00	0.0000
	Laser vs chemical	2.17	0.0434
S. sobrinus	Control vs laser	17.33	0.0000
	Control vs chemical	21.00	0.0000
	Laser vs chemical	3.67	0.0054

in pediatric orthodontics or long-term treatments where minimizing toxicity is critical [63]. These findings underscore the potential of GL13K-HAP-coated PEEK beads as safe and effective materials for orthodontic applications, offering both antibacterial protection and minimal risk of adverse cellular responses [64]. To our knowledge, this is the first study to demonstrate the successful coating of orthodontic PEEK beads with GL13K-HAP nanocomposites, showcasing both antibacterial properties and biocompatibility using eco-friendly laser methods. However, further research is needed to validate these results through in vivo studies and to explore the long-term interactions between the coated beads and oral tissues under dynamic clinical conditions.

5 Conclusion

This study demonstrated the potential of hydroxyapatite nanoparticles conjugated with the GL13K peptide (GL13K-HAP) as a novel antibacterial coating for orthodontic PEEK beads. The antibacterial efficacy of the coated beads was evident, with significant inhibition zones observed against both Gram-positive and Gram-negative bacterial strains, highlighting their capability to reduce bacterial colonization and mitigate the risk of enamel demineralization and white spot lesions during orthodontic treatments. Additionally, the biocompatibility of the coated beads, as demonstrated through cytotoxicity assays,

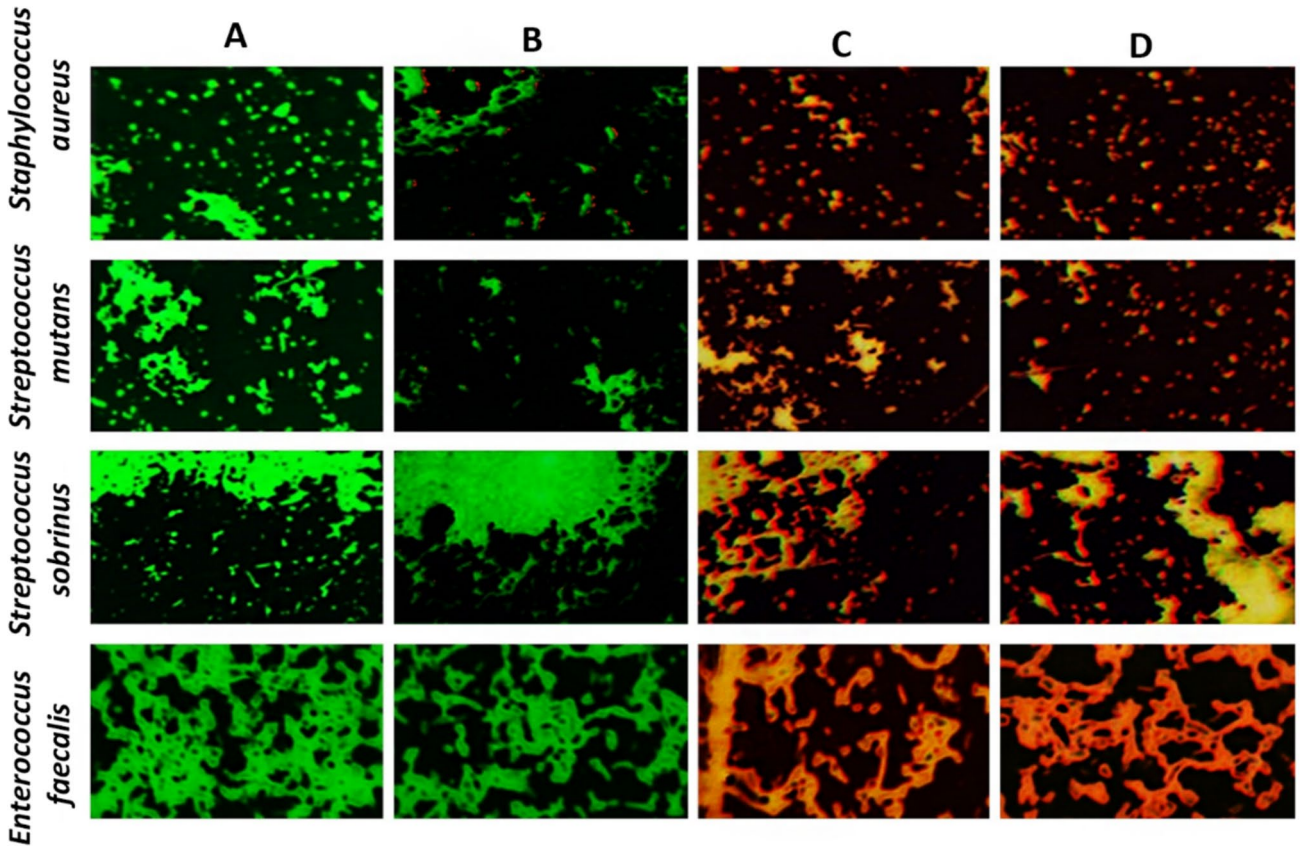

Fig. 17 Fluorescence microscopic images of the green and red fluorescence-stained. **A** Untreated bacterial strains. **B** Bacterial strains treated with the control material. **C** Bacterial strains treated with laser-prepared materials. **D** Bacterial strains treated with chemically prepared materials

underscores their safety for clinical applications. The high cell viability of REF cells upon exposure to the nanocomposite coatings indicates minimal adverse effects, with laser-prepared beads showing slightly superior biocompatibility due to the absence of chemical residues. The study also highlighted the advantages of incorporating nanotechnology into orthodontic materials, particularly the role of GL13K-HAP in promoting bacterial agglutination, enhancing phagocytic clearance, and reducing microbial adhesion without inducing bacterial resistance. These attributes, coupled with the mechanical and aesthetic benefits of PEEK as a substrate, position GL13K-HAP-coated PEEK beads as a transformative solution in orthodontic care. Future research should focus on in vivo validation of these findings, including the long-term stability, wear resistance, and biological interactions of the coatings in the dynamic oral environment. Although the FTIR, AFM, and FESEM analyses suggest stable immobilization of GL13K-HAP on the PEEK surface, further studies involving quantitative adhesion and release profiling under dynamic conditions are recommended to fully validate long-term coating stability. Additionally, optimizing the synthesis methods for scalability and investigating the coating's effects on diverse microbial communities will further enhance their clinical applicability. In conclusion, this study establishes GL13K-HAP-coated orthodontic PEEK beads as a promising material that combines antimicrobial efficacy with biocompatibility, offering a sustainable and innovative approach to addressing common complications in orthodontic treatments. This advancement not only improves patient outcomes but also represents a significant step forward in the development of smart, bioactive dental materials.

Supplementary Information The online version contains supplementary material available at https://doi.org/10.1007/s12668-025-02188-8.

Acknowledgements Not applicable

Authors' contributions The study was led by H.S. M-S, with key contributions from R.I.M in nanocomposite preparation, A.G in clinical applications, A.F.A in 3D design and milling, T.M.R in nanocomposite and antibacterial testing, J.R.A in biological contributions, manuscript drafting, and review, F.L.S in characterization and editing, and M.J in statistical and cytotoxicity analyses.

Funding Open access funding provided by The Ministry of Higher Education Malaysia and Universiti Pendidikan Sultan Idris.

Data Availability Raw data can be made available upon request

Declarations

Competing Interests The authors declare no competing interests.

Ethical Approval Not applicable.

Research Involving Humans and Animals Statement None.

Informed Consent None.

References

1. Höchli, D., Hersberger-Zurfluh, M., Papageorgiou, S. N., & Eliades, T. (2016). Interventions for orthodontically induced white spot lesions: A systematic review and meta-analysis. *European Journal of Orthodontics, 39*(2), 122–133. https://doi.org/10.1093/ejo/cjw065
2. Agrawal, A., & Shigli, A. (2012). Comparison of six different methods of cleaning and preparing occlusal fissure surface before placement of pit and fissure sealant: An in vitro study. *Journal of the Indian Society of Pedodontics and Preventive Dentistry, 30*(1), 51–55.
3. Al-Mamoori, R. M. H. J., & Al Haidar, A. H. M. J. (2022). Effect of resin infiltration and microabrasion on the microhardness of the artificial white spot lesions (an in vitro study). *Journal of Baghdad College of Dentistry, 34*(1), 44–50.
4. Shakir, M., Mohammed-Salih, H. S., Hussein, F. H., Al-Obaidi, J. R., & Supian, F. L. (2024). Innovation of nano-hydrogels loaded with amelogenin peptide and hydroxyapatite nanoparticles for remineralisation of artificially induced white spot lesions. *Journal of Drug Delivery Science and Technology, 99*, Article 105986. https://doi.org/10.1016/j.jddst.2024.105986
5. Rahee, S. S., & Jehad, R. H. (2023). Comparing the effectiveness of using three different re-mineralizing pastes on remineralisation of artificially induced white spot lesion. *Journal of Baghdad College of Dentistry, 35*(4), 35–45.
6. Gorr, S.-U., Sotsky, J. B., Shelar, A. P., & Demuth, D. R. (2008). Design of bacteria-agglutinating peptides derived from parotid secretory protein, a member of the bactericidal/permeability increasing-like protein family. *Peptides, 29*(12), 2118–2127. https://doi.org/10.1016/j.peptides.2008.09.019
7. Lemos, J. A., Palmer, S. R., Zeng, L., Wen, Z. T., Kajfasz, J. K., Freires, I. A., et al. (2019). The Biology of Streptococcus mutans. *Microbiology Spectrum, 7*(1).https://doi.org/10.1128/microbiolspec.gpp3-0051-2018
8. Merghni, A., Ben Nejma, M., Hentati, H., Mahjoub, A., & Mastouri, M. (2014). Adhesive properties and extracellular enzymatic activity of *Staphylococcus aureus* strains isolated from oral cavity. *Microbial Pathogenesis, 73*, 7–12. https://doi.org/10.1016/j.micpath.2014.05.002
9. Ahmed, S., Jehad Hassan, S., Gajdhar, S., Saleh Alhazmi, L., Yahya Khalifah, R., Alhusain Alrifai, J., et al. (2024). Prevalence of *Enterococcus faecalis* and *Candida albicans* in endodontic retreatment cases: A comprehensive study. *The Saudi Dental Journal, 36*(4), 539–545. https://doi.org/10.1016/j.sdentj.2024.01.009
10. Scaramucci, T., Carvalho, J. C., Hara, A. T., & Zero, D. T. (2015). Causes of dental erosion: intrinsic factors. In *Dental*

erosion and its clinical management (pp. 35–67). Springer, Cham. https://doi.org/10.1007/978-3-319-13993-7_3
11. Abduljawad, A., Mohammed-Salih, H., Jabir, M., & Almahdy, A. (2023). The effectiveness of a 10-methacryloyloxydecyl dihydrogen phosphate (10-MDP)-containing hydrophilic primer on orthodontic molar tubes bonded under moisture contamination: A randomized controlled trial. *Coatings*. https://doi.org/10.3390/coatings13091635
12. Kokubo, T. (2008). *Bioceramics and their clinical applications*. Elsevier.
13. Ramakrishna, S., Ramalingam, M., Kumar, T. S., & Soboyejo, W. O. (2016). *Biomaterials: Nano approach*. CRC Press.
14. Hussein, A. M., Mohammed-Salih, H. S., & Al-Sheakli, I. I. (2022). Effects of various cleaning agents on polypropylene and copolyester thermoplastic orthodontic retainer materials. *Journal of Taibah University Medical Sciences, 17*(5), 861–868. https://doi.org/10.1016/j.jtumed.2022.04.005
15. Abutayyem, H., Abdullatif Alshehhi, M., Alameri, M., & Sohail, Z. M. (2024). Microbial adhesion on different types of orthodontic brackets and wires: An in vitro study. *The Saudi Dental Journal, 36*(11), 1459–1465. https://doi.org/10.1016/j.sdentj.2024.09.004
16. Abdulaziz, S. M. (2018). Occurrence and pattern of antibiotic resistance among dental plaque bacteria from gingivitis patients and their clinical correlation. *Journal of Baglasdesh College of Dentistry., 30*(2), 12–234.
17. Barbieri, R., Coppo, E., Marchese, A., Daglia, M., Sobarzo-Sánchez, E., Nabavi, S. F., et al. (2017). Phytochemicals for human disease: An update on plant-derived compounds antibacterial activity. *Microbiological Research, 196*, 44–68. https://doi.org/10.1016/j.micres.2016.12.003
18. Salmerón-Valdés, E. N., Cruz-Mondragón, A. C., Toral-Rizo, V. H., Jiménez-Rojas, L. V., Correa-Prado, R., Lara-Carrillo, E., et al. (2022). Mechanical properties and antibacterial effect on mono-strain of *Streptococcus mutans* of orthodontic cements reinforced with chlorhexidine-modified nanotubes. *Nanomaterials*. https://doi.org/10.3390/nano12172891
19. Auconi, P., Caldarelli, G., Scala, A., Ierardo, G., Polimeni, A. J. O., Research C. (2011). A network approach to orthodontic diagnosis. *Orthodontics & Craniofacial Research, 14*(4), 189–197.
20. Mohammed-Salih, H. S., Ghazi, A., Mahmood, R. I., Al-Qazzaz, H. H., Supian, F. L., Al-Obaidi, J. R., et al. (2024). Enhancing orthodontic treatment control with fish scale-derived hydroxyapatite nanoparticles: Insights from an animal model study. *The Saudi Dental Journal, 36*(8), 1128–1134. https://doi.org/10.1016/j.sdentj.2024.06.007
21. Gamelas, J., & Martins, A. (2015). Surface properties of carbonated and non-carbonated hydroxyapatites obtained after bone calcination at different temperatures. *Colloids and Surfaces A: Physicochemical and Engineering Aspects, 478*, 62–70.
22. John, Ł, & Ejfler, J. J. P. (2023). A brief review on selected applications of hybrid materials based on functionalized cage-like silsesquioxanes. *Polymers, 15*(6), Article 1452. https://doi.org/10.3390/polym15061452
23. Dong, Y. (2023). Laser-assisted nanotexturing and silver immobilization on titanium implant surfaces to enhance bone cell mineralization and antimicrobial properties. Langmuir. 38(13). https://doi.org/10.1021/acs.langmuir.2c00008
24. Yu, D., Lei, X., & Zhu, H. (2022). Modification of polyetheretherketone (PEEK) physical features to improve osteointegration. *Journal Of Zhejiang University-Science B, 23*(3), 189–203. https://doi.org/10.1631/jzus.B2100622
25. Sukaimi, J. A. M. A. L. I., Hamzah, S. O. F. I. A. H., & Ghazali, M. S. M. (2015). Green synthesis and characterization of hydroxyapatite from fish scale biowaste. *Applied Mechanics and Materials*, *695*, 235–238. https://doi.org/10.4028/www.scientific.net/AMM.695.235
26. Panda, N. N., Pramanik, K., & Sukla, L. B. (2014). Extraction and characterization of biocompatible hydroxyapatite from fresh water fish scales for tissue engineering scaffold. *Bioprocess and Biosystems Engineering, 37*, 433–440.
27. Farooq, I., & Bugshan, A. J. F. (2020). The role of salivary contents and modern technologies in the remineralization of dental enamel: A narrative review. *F1000Research*. https://doi.org/10.12688/f1000research.22499.2
28. Kurtz, S. M., & Devine, J. N. (2007). PEEK biomaterials in trauma, orthopedic, and spinal implants. *Biomaterials, 28*(32), 4845–4869.
29. Schwitalla, A. D., Spintig, T., Kallage, I., & Müller, W.-D.J.D.M. (2015). Flexural behavior of PEEK materials for dental application. *Dental Materials, 31*(11), 1377–1384.
30. Schmidlin, P. R., Stawarczyk, B., Wieland, M., Attin, T., Hämmerle, C. H., & Fischer, J. JDm. (2010). Effect of different surface pre-treatments and luting materials on shear bond strength to PEEK. *Dental Materials, 26*(6), 553–559.
31. Wiesli, M. G. (2015). Özcan MJId. *High-performance polymers and their potential application as medical and oral implant materials: A review, 24*(4), 448–457.
32. Liu, D., Pourrahimi, A. M., Olsson, R. T., Hedenqvist, M., & Gedde, U. (2015). Influence of nanoparticle surface treatment on particle dispersion and interfacial adhesion in low-density polyethylene/aluminium oxide nanocomposites. *European Polymer Journal, 66*, 67–77.
33. Al-Ziaydi, A. G., Al-Shammari, A. M., Hamzah, M. I., Kadhim, H. S., & Jabir, M. S. (2020). Hexokinase inhibition using D-mannoheptulose enhances oncolytic newcastle disease virus-mediated killing of breast cancer cells. *Cancer Cell International, 20*, 1–10.
34. Hadi, N. A., Mahmood, R. I., & Al-Saffar, A. Z. J. G. R. (2021). Evaluation of antioxidant enzyme activity in doxorubicin treated breast cancer patients in Iraq: A molecular and cytotoxic study. *Gene Reports,24*, Article 101285.
35. Mahmood, R. I., Abbass, A. K., Al-Saffar, A. Z., & Al-Obaidi, J. R. (2021). An in vitro cytotoxicity of a novel pH-sensitive lectin loaded-cockle shell-derived calcium carbonate nanoparticles against MCF-7 breast tumour cell. *Journal of Drug Delivery Science and Technology, 61*, 102230.
36. Al-Rahim, A. M., Mahmood, R. I., Mohammed, M. M., & Omer, D. J. G. R. (2022). In vitro evaluation of antioxidant and cytotoxic activity of folate-methotrexate conjugated to bovine serum albumin nanoparticles against MCF-7. HepG2, and PC3 cell lines. *Gene Reports, 29*, Article 101666.
37. Ahmed, H., Ajat, M., Mahmood, R. I., Mansor, R., Razak, I. S. A., Al-Obaidi, J. R., et al. (2021). LC-MS/MS proteomic study of MCF-7 cell treated with dox and dox-loaded calcium carbonate nanoparticles revealed changes in proteins related to glycolysis, actin signalling, and energy metabolism. *Biology, 10*(9), Article 909.
38. Jawad, M., Öztürk, K., & Jabir, M. S. (2021). TNF-α loaded on gold nanoparticles as promising drug delivery system against proliferation of breast cancer cells. *Materials Today: Proceedings, 42*, 3057.
39. Al-Musawi, S., Albukhaty, S., Al-Karagoly, H., Sulaiman, G. M., Jabir, M. S., & Naderi-Manesh, H. JAi. N. S. N. (2020). Dextran-coated superparamagnetic nanoparticles modified with folate for targeted drug delivery of camptothecin. *Advances In Natural Sciences: Nanoscience And Nanotechnology, 11*(4), 045009.
40. Abbas, Z. S., Sulaiman, G. M., Jabir, M. S., Mohammed, S. A., Khan, R. A., Mohammed, H. A., et al. (2022). *Galangin/β-cyclodextrin inclusion complex as a drug-delivery system for improved solubility and biocompatibility in breast cancer treatment, 27*(14), 4521.

41. Al-Ziaydi, A. G., Al-Shammari, A. M., Hamzah, M. I., Kadhim, H. S., & Jabir, M. S. (2020). Newcastle disease virus suppress glycolysis pathway and induce breast cancer cells death. *Virusdisease., 31*(3), 341–348. https://doi.org/10.1007/s13337-020-00612-z
42. Lackington, W. A., Schweizer, P., Khokhlova, M., Cancellieri, C., Guimond, S., Chopard-Lallier, A.-L., et al. (2022). Femtosecond laser-texturing the surface of Ti-based implants to improve their osseointegration capacity. *Advanced Materials Interfaces, 9*(31), 2201164. https://doi.org/10.1002/admi.202201164
43. Ramanauskaite, L., & Snitka, V. (2015). The synthesis of controlled shape nanoplasmonic silver-silica structures by combining sol-gel technique and direct silver reduction. *Nanoscale Research Letters, 10*(1), 133. https://doi.org/10.1186/s11671-015-0839-x
44. Michalak, I., Mironiuk, M., & Marycz, K. (2018). A comprehensive analysis of biosorption of metal ions by macroalgae using ICP-OES, SEM-EDX and FTIR techniques. *PLoS One, 13*(10), Article e0205590. https://doi.org/10.1371/journal.pone.0205590
45. Ibrahim, I. M., Yunus, S., & Hashim, M. A. (2013). Relative performance of isopropylamine, pyrrole and pyridine as corrosion inhibitors for carbon steels in saline water at mildly elevated temperatures. *International Journal of Scientific Engineering and Research, 4*(2), 1–12.
46. Mecozzi, M., & Sturchio, E. (2017). Computer assisted examination of infrared and near infrared spectra to assess structural and molecular changes in biological samples exposed to pollutants: A case of study. *Journal Of Imaging, 3*(1), Article 11.
47. Hsieh, K.-H., Hsu, H.-C., Kao, Y.-L., Wu, S.-C., Yang, T.-Y., & Ho, W.-F. (2024). Nanohydroxyapatite/peptide composite coatings on pure titanium surfaces with nanonetwork structures using oyster shells. *Nanomaterials (Basel)*. https://doi.org/10.3390/nano14070577
48. Theerthagiri, J., Karuppasamy, K., Lee, S. J., Shwetharani, R., Kim, H.-S., Pasha, S. K. K., et al. (2022). Fundamentals and comprehensive insights on pulsed laser synthesis of advanced materials for diverse photo- and electrocatalytic applications. *Light, Science & Applications, 11*(1), Article 250. https://doi.org/10.1038/s41377-022-00904-7
49. Wang, Y., Hu, H., Jing, S., Wang, Y., Sun, Z., Zhao, B., et al. (2007). Enhanced raman scattering as a probe for 4-mercaptopyridine surface-modified copper oxide nanocrystals. *Analytical Sciences, 23*(7), 787–791.
50. Lasalvia, M., Scrima, R., Perna, G., Piccoli, C., Capitanio, N., Biagi, P., et al. (2018). Exposure to 1.8 GHz electromagnetic fields affects morphology, DNA-related raman spectra and mitochondrial functions in human lympho-monocytes. *PLoS ONE, 13*(2), Article e0192894.
51. Silva-Molina, R., Duarte-Moller, A., Orrantia-Borunda, E., Parra-Berumen, R. L., & Álvarez-Ramos, M. (2011). The role of pH on the second harmonic response of glycine sodium nitrate (GSN). *International Journal of the Physical Sciences, 6*(4), 885–890.
52. Pyrz, W. D., & Buttrey, D. J. J. L. (2008). Particle size determination using TEM: A discussion of image acquisition and analysis for the novice microscopist. *Langmuir, 24*(20), 11350–11360.
53. Predoi, D., Iconaru, S. L., Predoi, M. V., Groza, A., Gaiaschi, S., Rokosz, K., et al. (2020). Development of cerium-doped hydroxyapatite coatings with antimicrobial properties for biomedical applications. *Coatings*. https://doi.org/10.3390/coatings10060516
54. Sriprapha, P., Chokethawai, K., Randorn, C., Chandet, N., Thongkorn, K., Saenkam, K., et al. (2024). Induced porous structure with a slight change in mechanical properties of hydroxyapatite-based nanocomposites synthesized from waste bovine bone and their bioactivity. *Materials Today Sustainability, 26*, Article 100710. https://doi.org/10.1016/j.mtsust.2024.100710
55. Miculescu, F., Luță, C., Constantinescu, A. E., Maidaniuc, A., Mocanu, A.-C., Miculescu, M., et al. (2020). Considerations and influencing parameters in EDS microanalysis of biogenic hydroxyapatite. *Journal of Functional Biomaterials*. https://doi.org/10.3390/jfb11040082
56. Ozdal, M., & Gurkok, S. (2022). Recent advances in nanoparticles as antibacterial agent. *ADMET and Dmpk, 10*(2), 115–129.
57. Szwed-Georgiou, A., Płociński, P., Kupikowska-Stobba, B., Urbaniak, M. M., Rusek-Wala, P., Szustakiewicz, K., et al. (2023). Bioactive materials for bone regeneration: Biomolecules and delivery systems. *ACS Biomaterials Science & Engineering, 9*(9), 5222–5254. https://doi.org/10.1021/acsbiomaterials.3c00609
58. Delgado, A. H., & Young, A. M. (2021). Modelling ATR-FTIR spectra of dental bonding systems to investigate composition and polymerisation kinetics. *Materials*. https://doi.org/10.3390/ma14040760
59. Ortega-Martínez, J., Farré-Lladós, M., Cano-Batalla, J., & Cabratosa-Termes, J. (2017). Polyetheretherketone (PEEK) as a medical and dental material. A literature review. *Medical Research Archives, 5*(4). https://doi.org/10.18103/mra.v5i4.1209
60. Aktas, O. C., Puchert, K., Vurucu, E. E., Ersöz, B., Veziroglu, S., & Sen, S. (2024). A review on nanocomposite coatings in dentistry. *Journal Of Materials Science, 59*(38), 17991–18008. https://doi.org/10.1007/s10853-024-09915-8
61. Ramburrun, P., Pringle, N. A., Dube, A., Adam, R. Z., D'Souza, S., & Aucamp, M. (2021). Recent advances in the development of antimicrobial and antifouling biocompatible materials for dental applications. *Materials*. https://doi.org/10.3390/ma14123167
62. Okasha, A. T., Abdel-Khalek, A. A., Rudayni, H. A., Al Zoubi, W., Alfassam, H. E., Allam, A. A., et al. (2023). Synthesis and characterization of Mg-hydroxyapatite and its cellulose hybridized structure as enhanced bio-carrier of oxaliplatin drug; Equilibrium and release kinetics. *RSC Advances, 13*(43), 30151–30167. https://doi.org/10.1039/D3RA04268E
63. Mohammed-Salih, H. S., Ghazi, A., Mahmood, R. I., Al-Qazzaz, H. H., Supian, F. L., Al-Obaidi, J. R., et al. ((2024)). Enhancing orthodontic treatment control with fish scale-derived hydroxyapatite nanoparticles: Insights from an animal model study. *The Saudi Dental Journal*. https://doi.org/10.1016/j.sdentj.2024.06.007
64. He, L., Zhang, W., Liu, J., Pan, Y., Li, S., & Xie, Y. (2024). Applications of nanotechnology in orthodontics: A comprehensive review of tooth movement, antibacterial properties, friction reduction, and corrosion resistance. *BioMedical Engineering OnLine, 23*(1), 72. https://doi.org/10.1186/s12938-024-01261-9